

Analysis for the Robotic Assembly of Large Flexible Space Structures

by

Vickram S. Mangalgi

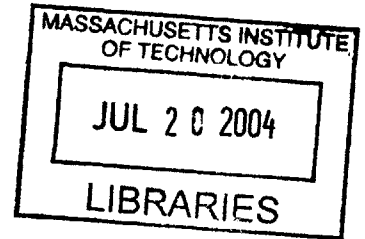
B. Tech. (Honors), Mechanical Engineering
Indian Institute of Technology – Kharagpur, 2001

Submitted to the Department of Mechanical Engineering
in Partial Fulfillment of the Requirements for the Degree of
Master of Science in Mechanical Engineering

at the

Massachusetts Institute of Technology

LIBRARY
January 2004



© 2004 Massachusetts Institute of Technology
All Rights Reserved

Signature of Author.....

Department of Mechanical Engineering
January 16, 2004

Certified by.....

.....
Steven Dubowsky
Professor of Mechanical Engineering
Thesis Supervisor

Accepted by.....

.....
Ain A. Sonin
Chairman, Department Committee on Graduate Students

BARKER

Analysis for the Robotic Assembly of Large Flexible Space Structures

by

Vickram S. Mangalgi

Submitted to the Department of Mechanical Engineering
on January 16, 2004 in Partial Fulfillment of the
Requirements for the Degree of
Master of Science in Mechanical Engineering

ABSTRACT

Space solar power is a renewable, environment-friendly alternative to satisfy future terrestrial power needs. Space solar power stations will need to have large dimensions (on the order of hundreds of meters) to be able to collect enough power to make them cost effective. It will be infeasible to transport these large structures, fully assembled, from earth to space, or use human astronauts for their construction in space, leaving robotic assembly as the only viable option. The focus of the current work is to identify potential challenges to the large structure assembly process in space and develop methods to address them.

One of the major causes of failure in the assembly process would be dimensional mismatch between the two structures to be joined. The first part of this thesis analyses the static and dynamic effects on a typical large space structure using finite element models and predicts the deformation that the structure will undergo due to thermal and vibration effects in space. Forced assembly methods using cooperative robots are developed to compensate for these dimensional errors.

The second part of the thesis deals with the application of forced assembly methods to representative assembly scenarios. The scenarios are categorized based on the nature of the deformation involved. The differences between the use of thrusters and manipulators by robots are discussed and assembly plans are developed for each scenario using either or both types of actuators. A genetic algorithm based planner is developed and implemented to optimize the assembly process within the limits of the assumptions made.

Thesis Supervisor: Steven Dubowsky
Title: Professor of Mechanical Engineering

ACKNOWLEDGEMENTS

The research in the area of large space structures has turned out to be extremely challenging and with a measure of uncertainty. There are a number of people who have been instrumental in bringing this piece of work together. First and foremost, I would like to thank the Japan Aerospace Exploration Agency (JAXA) for supporting this research. Next, I would like to thank my advisor Dr D for his guidance and for giving me this opportunity. A special thanks to Vivek and Karl at the Field and Space Robotics Laboratory, MIT for their support and contributions. Thanks are also due to my colleagues in the Department of Mechanical Engineering, MIT for their patience in discussing my ideas. I am grateful to the NASDA/JAXA group at FSRL for bearing with me during the innumerable meetings and discussions and also to the visiting researchers from JAXA, Shuichi and Takeshi for their inputs. Last, but not the least, I would like to thank my family, room-mate and friends for supporting me through the difficult times during this two-year period.

CONTENTS

ABSTRACT	2
ACKNOWLEDGEMENTS.....	3
CONTENTS	4
FIGURES	6
TABLES	8
1 INTRODUCTION	9
1.1 Space Solar Power Stations (SSPS).....	9
1.2 Robotic Assembly of Large Space Structures (LSS).....	13
1.3 Literature Review.....	15
1.4 Thesis Outline	18
2 MODELING ASSEMBLY OF LARGE SPACE STRUCTURES	19
2.1 Approach to LSS Assembly.....	19
2.2 Inputs.....	21
2.2.1 Model Assumptions	21
2.2.2 Robot Model	23
2.3 Detailed Structural Analysis	24
2.3.1 Thermal Warping.....	25
2.3.2 Vibration Analysis	30
2.4 Assembly Methods.....	33
2.4.1 Cooperative Robots.....	33
2.4.2 Forced Assembly by Robot Manipulation	34
2.4.3 Thrusters for Assembly.....	39
2.5 Summary	40
3 ASSEMBLY STRATEGIES.....	41
3.1 Optimal Assembly Planning	41
3.1.1 Numerical Optimization Methods.....	41
3.1.2 GA-based Optimal Approach to Assembly	47
3.1.3 Optimal Robot Pose	52
3.2 Inputs.....	54
3.3 Small Scale Deformation Scenarios.....	56
3.3.1 Single Connection Point	56
3.3.2 Multiple Connection Points	58
3.3.3 Flexible LSS.....	62

3.4	Large Scale Deformation Scenarios.....	65
3.4.1	Single Connection Point	65
3.4.2	Multiple Connection Points	72
4	CONCLUSIONS AND FUTURE DIRECTION	75
4.1	Conclusions.....	75
4.2	Future Direction	76
	REFERENCES	79
	APPENDIX A LARGE SPACE TRUSS MODEL	84
	APPENDIX B OPTIMAL ROBOT POSE	87

FIGURES

Figure 1.1: Space Solar Power Station concepts	10
Figure 1.2: Village of Grand-Bassin as seen from the location considered for microwave projectors.....	11
Figure 1.3: Large Solar Power Station construction scenario.....	14
Figure 1.4: LSS assembly steps	14
Figure 2.1: Approach to LSS Assembly	20
Figure 2.2: Large space truss model in ADINA	22
Figure 2.3: Robot Model for Assembly	23
Figure 2.4: Fully deployed ABLE Mast - ADAM™	24
Figure 2.5: Heat transfer in a semi-infinite beam	26
Figure 2.6: Simulating the thermal loads on a 3-D element (axes not to scale)	28
Figure 2.7: Thermal deformation of a triangular structure in space	29
Figure 2.8: Various vibration modes of a typical large truss.....	30
Figure 2.9: LSS impulse response	32
Figure 2.10: Forced deformation to desired shape (exaggerated for effect).....	35
Figure 2.11: Force analysis setup in ADINA.....	37
Figure 2.12: Large space truss bent back into shape under application of forces	37
Figure 2.13: Comparison of actual shape of the truss based on predicted forces with the desired shape.....	38
Figure 2.14: General Thrust Profile for Gas-Jet Control Systems.....	40
Figure 3.1: Utility of applying a force in the cost function	43
Figure 3.2: Force optimization algorithm	44
Figure 3.3: Optimal bending of a beam element.....	45
Figure 3.4: 3D plot of error in bending a beam vs force magnitude and location. Beam bending is computed analytically as well as using a finite element model.....	46
Figure 3.5: Shape error variation with number of robots.....	47

Figure 3.6: Node locations for force application on triangular truss	49
Figure 3.7: Determining the optimal robot pose for assembly	53
Figure 3.8: Optimal pose for maximum force output (plotted for different T1).....	53
Figure 3.9: Taxonomy of assembly scenarios.....	55
Figure 3.10: Assembly plan for the single connection point assembly case	57
Figure 3.11: Assembly with multiple connection points	58
Figure 3.12: Change in shape error for triangular truss bending with number of robots.....	59
Figure 3.13: Equi-distant spacing vs Chebyshev spacing.....	60
Figure 3.14: Shape error for beam bending – Equi-distant vs Chebyshev spacing	61
Figure 3.15: Effect of multiple connection points on truss stiffness	61
Figure 3.16: Comparing stiffness of triangular truss and base truss.....	63
Figure 3.17: Vibrations of the mating point after connection.....	64
Figure 3.18: Assembly for large scale deformation with single connection point	65
Figure 3.19: Finite Element Model of Small Truss Bent using Thrusters	66
Figure 3.20: Variation in shape error of triangular truss for force application anywhere on the truss.....	68
Figure 3.21: Simultaneous deformation for assembly using multiple robots	69
Figure 3.22: Determining Optimal Force Combination for Bending Small Truss	71
Figure 3.23: Assembly with multiple connection points	72
Figure 3.24: Minimum number of robots required to connect at given connection points on each beam of the truss	74
Figure 3.25: Variation of error with increasing number of robots used for assembly (2 connection points per beam).....	74
Figure 4.1: The LSS transportation problem – minimize vibrations and energy loss	78
Figure A.1: Thermal deformation of a large space truss	85
Figure A.2: Truss points generated for the large space truss in MATLAB using data obtained from thermal analysis of a smaller truss in ADINA	86
Figure B.1: Robot with two single-link arms.....	87
Figure B.2: Free body diagrams of the arms and body of the robot	88

TABLES

Table 1.1: Large Space Structures – A Comparison.....12

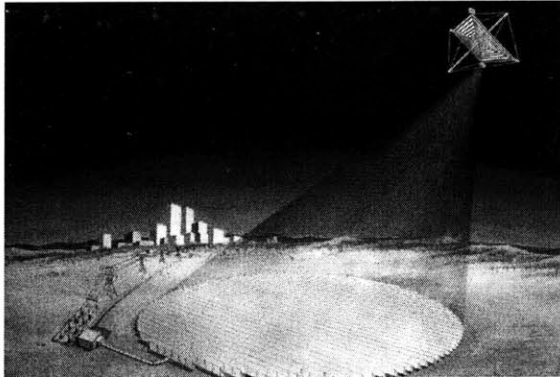
Table 2.1: SRTM ADAM™ Properties25

Table 2.2: Deformation and forces required for assembly for different truss shapes.....35

1.1 Space Solar Power Stations (SSPS)

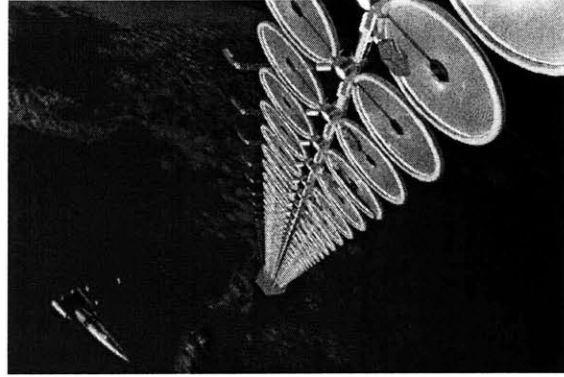
There has been considerable interest in developing alternative energy generation methods to meet the needs of the ever-increasing world population. The existing technology in power generation relies heavily on fossil fuels, which not only pollute the environment but also are limited in supply. Space solar power (SSP) has the potential of emerging as a clean, environment friendly alternative of the future to satisfy terrestrial power needs. The concept of exceptionally large solar power satellites (SPS) that beam energy down to the earth was first proposed by Dr Peter Glaser of Arthur D. Little [Glaser, 1976]. Since then, the SPS designs have evolved with time and organization. Some SPS designs developed by NASA and the Japan Aerospace Exploration Agency – JAXA (formerly NASDA) are shown in Figure 1.1. Figure 1.1a illustrates the Rectenna [Brown, 1984] in which SPS power is beamed to a receiving antenna or "rectenna" on Earth through microwaves. The rectenna converts the microwave energy back into electrical current, which is fed into the power grid. The power beam would be safe for insects and birds flying through, and would not reach plant life growing under the rectenna. Figure 1.1b is the NASA *Sun Tower* SPS concept [Mankins, 2002] that has emerged from the ambitious SSP Exploratory Research and Technology (SERT) Program. The discs shown are lightweight, inflatable fresnel reflectors that focus the sun's radiation onto photovoltaic cells. One of the 1999 SPS designs proposed by JAXA

comprises of C60 type modularized solar batteries arranged to minimize the effect of shadows (shown in Figure 1.1c). The 2001 NASDA reference model comprises of a primary and secondary reflection mirror (or lens) along with a power generation and transmission module (Figure 1.1d) [Matsumoto, 2001]. Duke et al. [2001] also go as far as proposing to build photovoltaic energy collection systems on the moon, the energy from which could be used for applications in space as well as beamed to the earth.



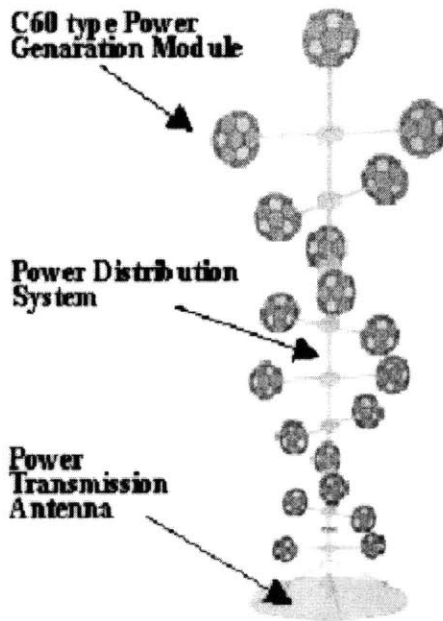
Credit: Space Studies Institute

a: Rectenna

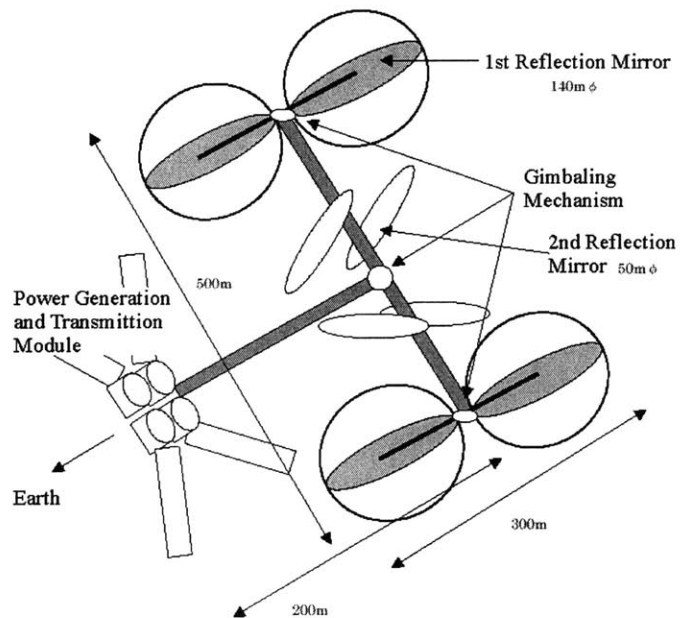


Credit: NASA artwork by Pat Rawlings/SAIC

b: NASA SunTower SPS concept



c: NASDA's 1999 Model of 10 MW Experimental SSPS



Credit: NASDA / JAXA

d: 2001 Baseline Model of NASDA's 10 MW Experimental SSPS

Figure 1.1: Space Solar Power Station concepts



Figure 1.2: Village of Grand-Bassin as seen from the location considered for microwave projectors

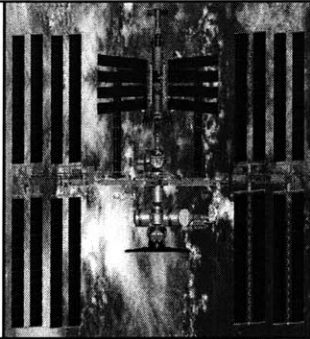
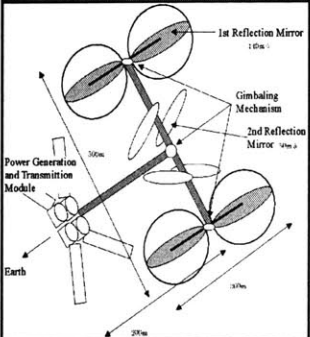
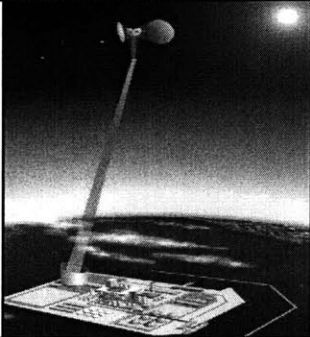
Wireless Power Transmission (WPT) methods have been explored to transmit this power generated in space to earth with minimal environmental impact. These include the use of microwave as well as visible light transmission. The implementation of ground based WPT systems and their effect on the environment will be studied in the Grand Bassin project (Figure 1.2) [Pignolet et al., 2001].

Since the energy density corresponding to solar power is rather low, the SSP systems need to have dimensions spanning several kilometers to deliver power comparable to existing power plants. Typically an SPS of dimensions 5 km by 10 km in area would be required for a system delivery of 5 GW to the ground. This would certainly be the largest space structure ever to be built. A comparison between existing and proposed space structures with respect to their dimensions, mass and time to build has been made in Table 1.1.

It follows that building such huge structures on earth and transporting them to space or constructing them by astronauts performing EVA, will not be feasible. The in-space assembly will typically be carried out in the geosynchronous earth orbit (GEO) although initial prototypes may be built in the low earth orbit (LEO). This leaves robotic assembly as the only viable option. Hundreds of intelligent robots working at a fairly

autonomous level of control would be required to perform complex tasks relating to assembly, inspection and also maintenance at a later stage. These free-flying robots would operate in a cooperative manner with limited resources at their disposal to carry out the construction.

Table 1.1: Large Space Structures – A Comparison

	<p>MIR Dimensions: 33m x 30m x 27m Total mass: 120 tons Time to build: 10 years</p> <p><i>Credit: Russian Space Agency</i></p>		<p>ISS Dimensions: 88m x 109m x 40m Total mass: 470 tons Time to build: 5 years</p> <p><i>Credit: NASA</i></p>
	<p>10MW NASDA Experimental SSPS Dimensions: 500m x 350m x 150m Total mass: 500 tons Time to build: ?</p> <p><i>Credit: NASDA / JAXA</i></p>		<p>1GW NASDA Business Model of SSPS Dimensions: 15km x 12km x 5km Total mass: ~10⁶ tons Time to build: ?</p> <p><i>Credit: NASDA / JAXA</i></p>

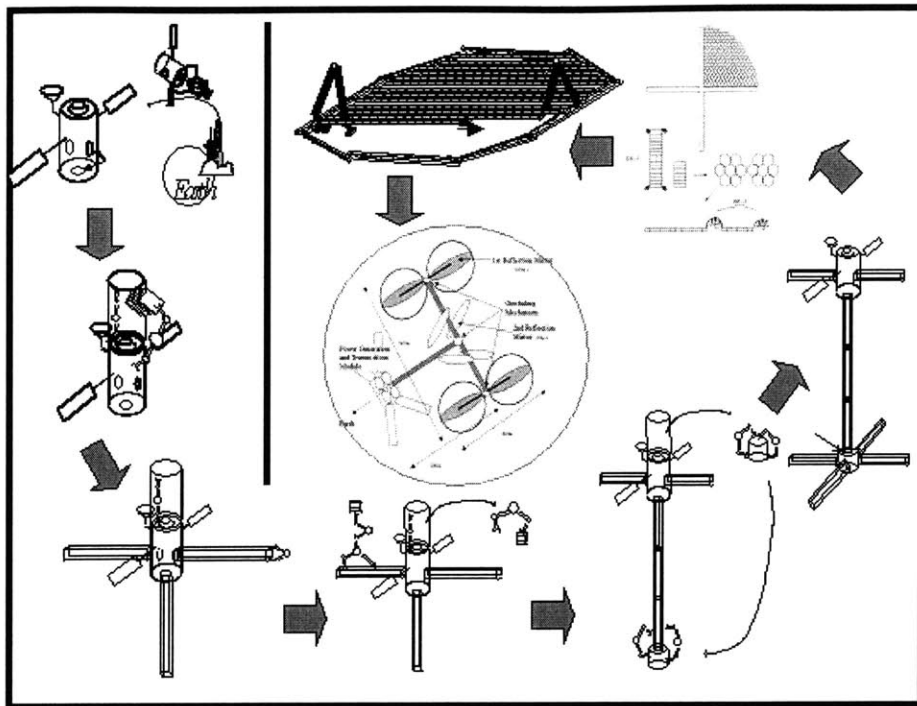
Typical assembly tasks would involve transportation, path planning, cooperation between robots and information collection and sharing, while taking into account the conditions of the working environment. These are unexplored areas of research and need to be studied in-depth to ensure the success of the mission. The focus of this thesis is to identify potential problems that may affect the large space structure assembly process in space and develop methods to solve them.

1.2 Robotic Assembly of Large Space Structures (LSS)

The construction and assembly of large structures in space is a challenging task that requires multiple robots working cooperatively. A typical construction scenario is shown in Figure 1.3. An Earth-to-Orbit (ETO) launch vehicle transports the payload to the LEO or GEO. Here a construction site is chosen and cooperative teams of robots perform the assembly. This may involve the following general tasks:

- Building long elements – This would be the first step in which compact stacks composed of high stiffness composite struts, metallic fittings and precision ball joints would be deployed to form a long truss structure.
- Assembling elements in a sub-structure – These modules would form basic building blocks for the final assembly. Depending on the design of the final structure these could be single beams, triangular, honeycomb-like or polygonal in shape (Figure 1.4a). This assembly process would not be constrained by the dimensions of other members.
- Transportation and Maneuvering – Multiple free-flying cooperative robots would be used to carry out the task of transportation of components from the shuttle to the module construction site and of the assembled modules to their final location on the structure. Various factors like vibration suppression, actuation limitations and limited sensing capabilities of the robots would have to be taken into account.
- Assembling the sub-structures to form the LSS – As shown in Figure 1.4b, this final assembly process would be the equivalent of fitting pieces in a jig-saw puzzle in that it would be constrained by the dimensions of the structure already built. Robots would collectively maneuver the modules and connect them to the base structure using latching mechanisms.

Any significant variation in dimensions from the designed values would lead to incompatibilities in the assembly process. Various factors that cause this dimensional mismatch need to be explored to get an estimate of the variation. Effective methods for compensation of such changes in dimension need to be developed to successfully carry out the assembly.



Credit: Shuichi Matsumoto, NASDA 2001

Figure 1.3: Large Solar Power Station construction scenario

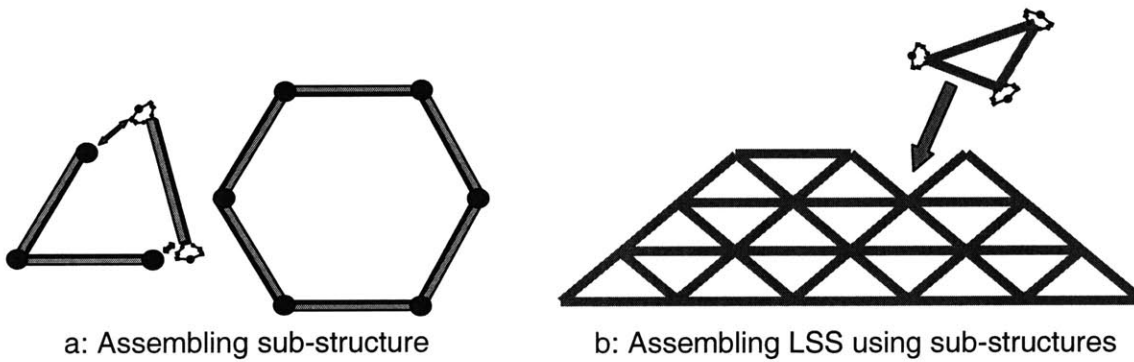


Figure 1.4: LSS assembly steps

1.3 Literature Review

Various space organizations across the world have been involved with the concept study for a space solar power station which has led to considerable interest in the area of large space structure assembly using autonomous robots. NASA's SERT and SCTM (SSP Concepts & Technology Maturation) programs have focused on developing intelligent robotics to carry out assembly with minimal use of humans [Mankins, 2002]. JAXA and other agencies in Japan have been studying tele-operation technologies for controlling space robots. Experiments have been carried out using the Engineering Test Satellite VII (ETS-VII), which is a robotic satellite equipped with six degree-of-freedom manipulators and antenna assembling mechanisms developed by the Communication Research Laboratory (CRL) [Kimura et al., 1999, Oda, 2000]. Europe has also been very active in developing space robotics for missions such as servicing geo-stationary satellites and in-orbit assembly of large space structures [Putz, 1998]. These programs have delved extensively into the costs involved in the SSP construction mission and looked at ways to reduce the costs to make it economically feasible.

Given the status of research in the area of robotic construction of large space structures, it is clear that current technology cannot fulfill the requirements of on-orbit construction. Ueno et al. [1997] highlighted three key technological hurdles that need to be overcome for on-orbit construction to become a reality. These are teleoperation with limitations such as sensing and communication delays, stable contact with objects using manipulators and the problem of three-dimensional mobility in a free-floating environment. Whittaker et al. [2001] examined the technical challenges facing the use of free-flying robot, fixed-base manipulators and attached mobile manipulators for the space structure construction process. The relative advantages and disadvantages in using each kind of device are brought out. Free-flying robots would typically be used for the inspection process. The Autonomous Extravehicular Robotic Camera (AERCam) is a free-flying camera platform that has been flight tested. In an experiment in December 1997, the robot was able to provide the astronauts with space shuttle images from various angles and distances. Lichter and Dubowsky [2003] developed a technique to estimate the state, shape, and inertial parameters of space objects from sequences of range images

that could be obtained from the AERCam. The technique uses kinematic data fusion to condense raw sensory data into a coarse estimate of the target pose and applies Kalman filtering to extract the full time dynamic state of the object. The target shape estimates can be compared with the structural model of the object to further refine the estimate.

Dexterous free flying robots like the Ranger are suited to perform a variety of space structure construction tasks. Prototypes of the Ranger like the Ranger Neutral Buoyancy Vehicle (NBV) have been successfully tested in water tank experiments. Various fixed base manipulators like the Remote Manipulator System on the International Space Station (ISS) have been used to perform a variety of material handling and repair operations in space and could provide the technological foundation for the eventual goal of carrying out robotic construction.

Coppa [1995] developed an automated approach to space truss construction, particularly of the Coppatruss system. A robotic assembly process will feed frames and struts to automatically assemble truss elements with square and triangular cross-sections. Rule and Thomas [1994] described a preliminary design concept for a welded joint to be used in on-orbit assembly and looked at the thermal stresses that would be set up in the joint due to the effects of differential thermal expansion.

Way and Olds [2001] develop the concept of Swarm, which is a solar-electric orbital transfer vehicle. Swarm will be used to deploy elements of space structures and will be delivered to the construction site in space aboard a reusable launch vehicle. Once it reaches the construction site, the entire vehicle will be disassembled and used as part of the construction material. A cost-benefit analysis, however, does not justify the use of Swarm and further improvements are necessary.

The environment conditions in space will be extremely harsh and space structures would have to be well-protected against fluctuations in thermal conditions. Malla et al. [1988] have studied the radiation thermal effects on the attitude motion, orbital motion and static deformation of a large space structure. There are three major sources of heat in space – direct solar radiation, direct Earth radiation and Earth’s albedo. The thermal effects due to the Earth are found to be significant on structures closer to the Earth in the Low Earth Orbit (LEO). However, in high altitude orbits like the GEO, these effects may be neglected. The orbital motion of these structures in and out of the Earth’s shadow will

also affect them especially if they are closer to the Earth. An example of the kind of problems that thermal effects will cause in space is the low frequency vibration induced in the solar panels of the Hubble Space Telescope. If ignored, these thermal effects are likely to cause mission failure.

The use of robot actuators to control the shape of a truss that has been thermally deformed is developed later in this text. Agrawal and Treanor [1999] used piezoelectric actuators to control the shape of a beam. Optimum actuator locations and voltage conditions can be determined by minimizing the error between the desired shape and the achieved shape.

1.4 Thesis Outline

This thesis presents analysis for the assembly of large space structures using cooperative robots. The main problem addressed is that of assembly of structures with dimensional mismatch. This work was done as part of a collaborative effort between the MIT Field and Space Robotics Laboratory and JAXA. The basic objective of this research program was to provide research and development support to JAXA in its mission to construct large solar power stations. As a part of this work, important tasks regarding large space structure construction were identified, research themes based on these tasks were defined and methods were developed to solve some of the problems associated with it.

The thesis is organized into three main parts. The first part develops structural models for large space structures to analyze the effects of the harsh environment in space. The problem of dimensional mismatch is explained and forced assembly methods are developed. The second part deals with the assembly problem involving small and large scale deformation. Assembly plans involving cooperative robots are developed based on the scenario assumptions and conditions. The final chapter summarizes the major results of this thesis and recommends directions for future work in this area.

MODELING ASSEMBLY OF LARGE SPACE STRUCTURES

2.1 Approach to LSS Assembly

The assembly of large space structures can be categorized into various assembly tasks. A basic methodology is developed to carry out these tasks. Each task can be divided into three main steps (see Figure 2.1):

- (i) Determining the Inputs – This is information about the structure and resources available, which will include structural shape, size and properties and models of the sensors and actuators to be used.
- (ii) Feeding the Inputs to the Assembly Planner – This step involves detailed structural analysis that gives estimates of thermal warping and vibrations in the structure due to external disturbances. Based on the nature of the deformation, different methods of assembly by deformation, reconfiguration or timing of the assembly process are analyzed.
- (iii) Determining the Outputs – The most suitable method for carrying out the assembly process is recommended depending on the inputs. The recommendation includes information about number of robots to be used, assembly strategies, forces applied and deformations that would occur in the large space structure, and the resulting structural vibrations.

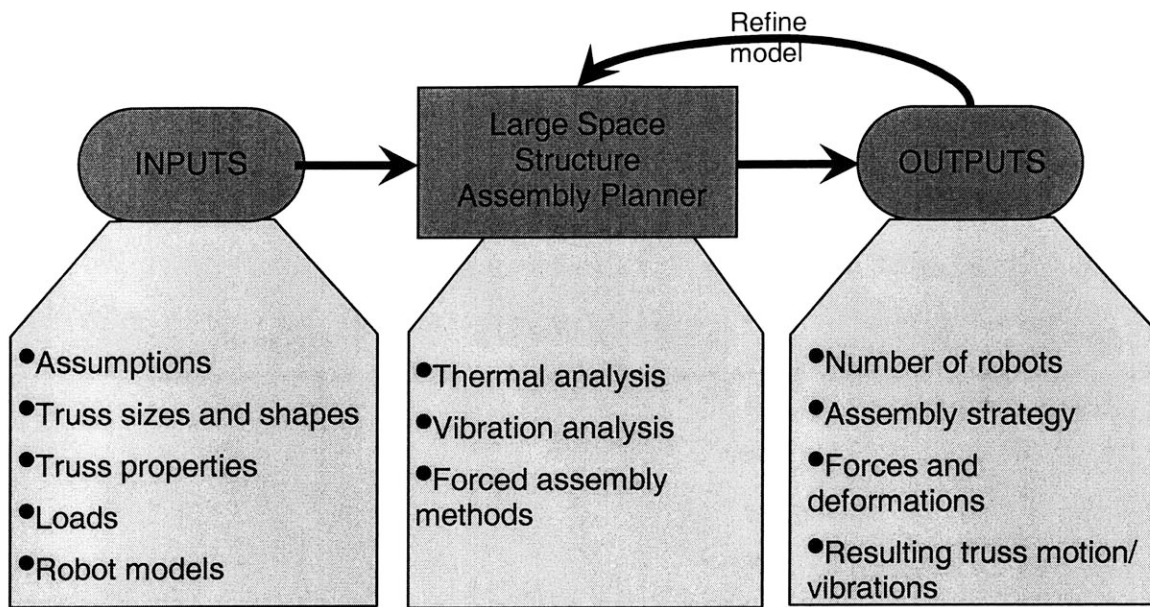


Figure 2.1: Approach to LSS Assembly

2.2 Inputs

2.2.1 Model Assumptions

Given the pioneering nature of the large space structures mission, it is essential to base the research on reasonable assumptions regarding various parameters involved. These assumptions are based on current and extrapolated data from existing systems. The large space structure is assumed to be of the order of a few kilometers in dimension and having a modular construction pattern. Assumptions are also made regarding the available resources to carry out the assembly process including actuator and sensor limitations of robots. Some of these are listed below:

- A thin, large, sheet-like structure having planar dimensions of about 2 km x 2 km and thickness of 1m (referred to as the ‘base truss’) already exists in space. The base truss is located in the geosynchronous earth orbit (GEO).
- This base truss is made up entirely of smaller triangular shaped truss elements (referred to as the ‘small truss’ or ‘triangular truss’) 200m long and having a one meter square cross-section. Base truss construction is incomplete and several small trusses need to be assembled on it (see Figure 2.2).
- All structures in space experience thermal deformation due to incident radiation from the sun.
- In high orbits like GEO, direct radiation from earth as well as earth’s albedo can be neglected. Heat flux changes due to the structure moving in and out of the earth’s shadow can also be neglected [Malla et al., 1988].
- Static deformation and dynamic effects on the large structure caused due to gravity in a high orbit like GEO are neglected.
- All joint connections are assumed to be rigid.

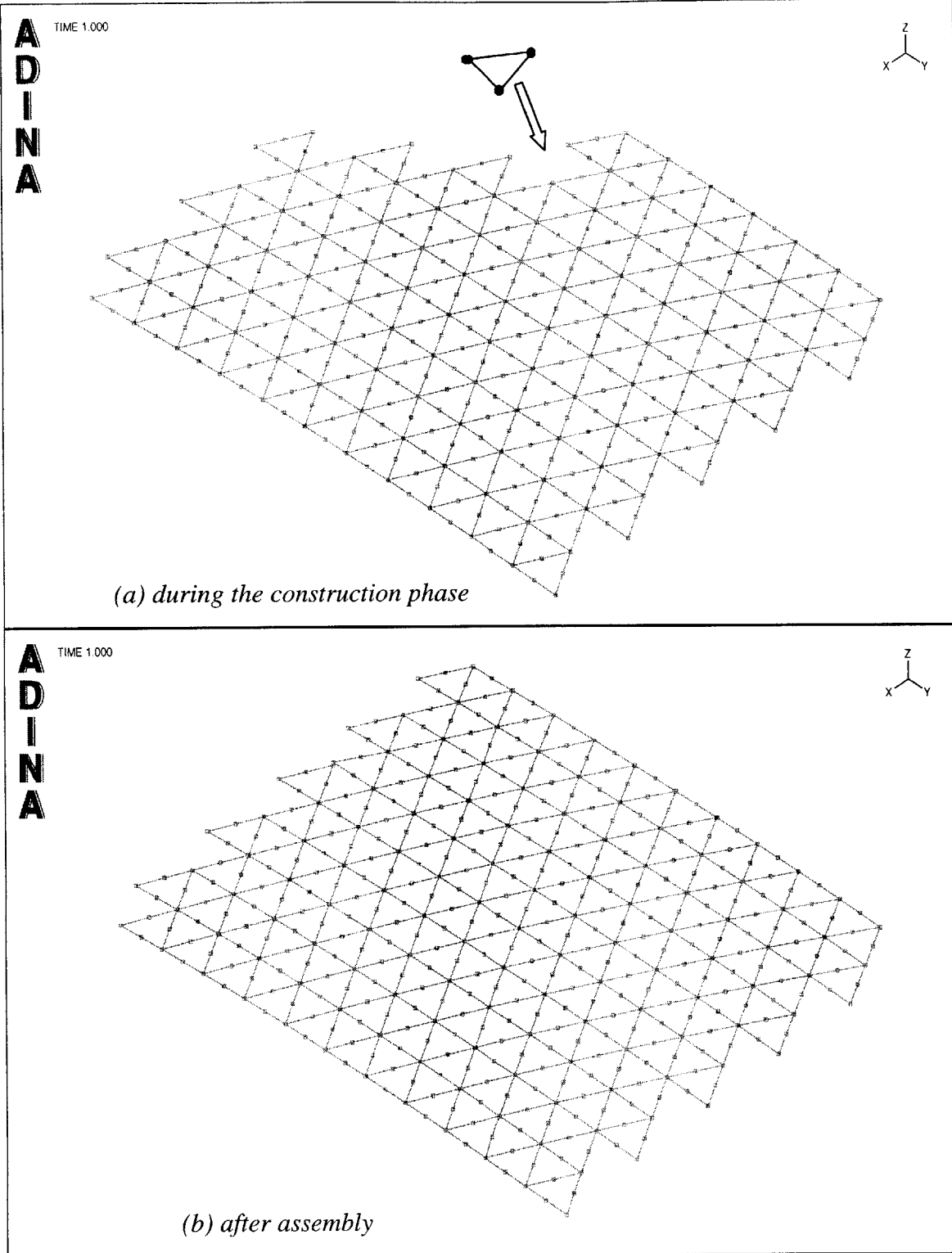


Figure 2.2: Large space truss model in ADINA

2.2.2 Robot Model

A representative robot model has been developed for the assembly problem based on the robot arm on the ETS-VII satellite and the JEMRMS [Ohkami, 1999]. The assembly robot used as a basis for work in this thesis has been shown in Figure 2.3. This robot consists of two 1.5 meter long arms with a mass of 25 kg each and a main body with a mass of 50 kg. The main body houses all the electronics including cameras, GPS receiver, onboard computer, communication system, docking system as well as thrusters and fuel. The robot is capable of applying a maximum force and torque of 30 N and 50 Nm, respectively, using its manipulators. It is also equipped with hydrazine or cold-gas-jet thrusters. These thrusters can apply forces in a free-floating environment of 1N for the cold-gas-jet type and up to 50N for the hydrazine type.

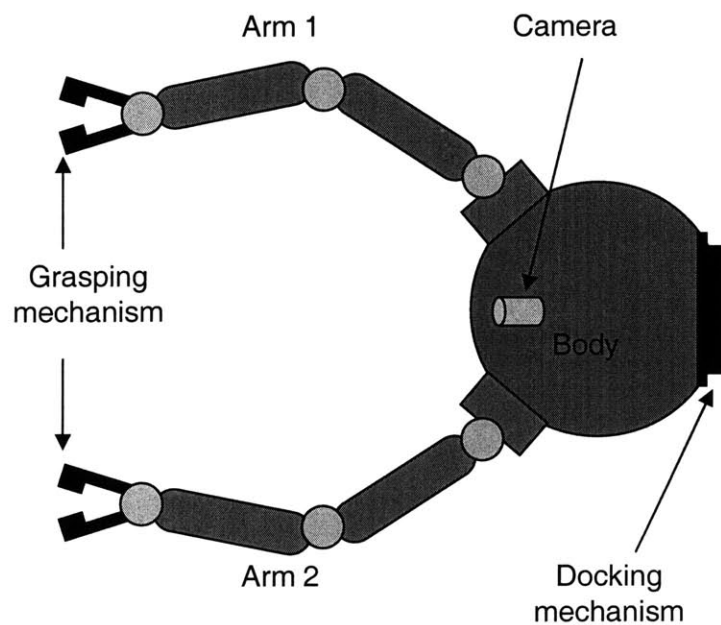
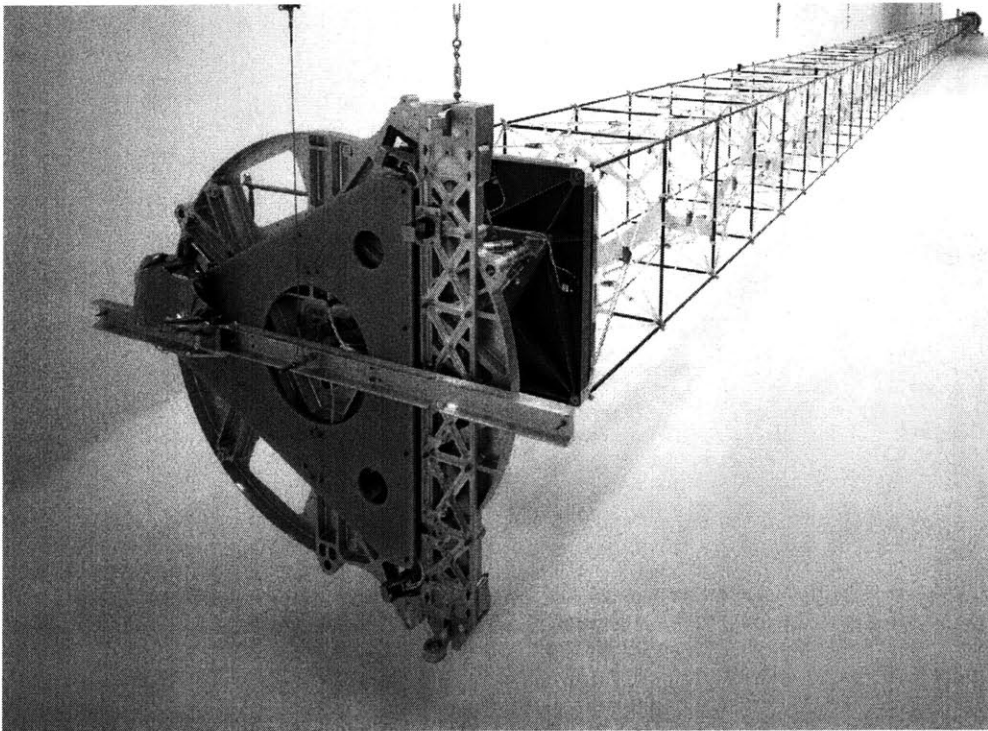


Figure 2.3: Robot Model for Assembly

2.3 Detailed Structural Analysis

As described earlier, the large space structures proposed for the SPS consist of massive sheet-like panels that reflect radiation from the sun onto a power generation module. To predict problems that may arise during the construction process, a detailed study was carried out on the structural change that these structures would undergo due to varying thermal conditions. The thermal effects will manifest themselves in the change of dimensions of these large structures, which need to be taken into account before successful assembly operations can be performed. The goal here is to provide an estimate of such dimensional changes.



Credit: AEC-Able Engineering Company, Inc.

Figure 2.4: Fully deployed ABLE Mast - ADAM™

2.3.1 Thermal Warping

The varying and harsh thermal conditions in space will affect the large structures by changing their dimensions and causing warpage. These effects have been studied and modeled on some representative structures using finite element analysis. The goal here is to provide an estimate of such dimensional changes. The basic building blocks are assumed to be deployable truss beams like the Able Articulated Deployable Mast (ADAMTM) [Gross et al.] (Figure 2.4). ADAMTM, made by the AEC-Able Engineering Company, has been successfully used on the International Space Station to deploy solar arrays and for the Shuttle Radar Topography Mission (SRTM) [Umland et al., 2001]. These individual beams, although truss-like in nature, are modeled as 3-D solid bodies. Material properties are back calculated from the ADAMTM specifications regarding thermal and mechanical stability. This technique facilitates the modeling of relatively complex structures made using these beams. See Table 2.1 for a list of mechanical properties of the SRTM ADAMTM.

Table 2.1: SRTM ADAMTM Properties

Strength and Stiffness		
Moment Strength M_{cr}	8140 Nm	
Shear Strength V_{cr}	400 N	
Torsional Strength T_{cr}	305 Nm	
EI (Bending)	$1.6 \times 10^7 \text{ Nm}^2$	
GA (Shear)	$4.9 \times 10^5 \text{ N}$	
GJ (Torsion)	$1.7 \times 10^5 \text{ Nm}^2$	
First Bending Mode (On-Orbit)	0.1 Hz	
First Torsion Mode (On-Orbit)	0.21 Hz	
Parametric Stability		
Degree of Freedom	Mechanical	Thermal
Length	$\pm 0.6 \mu\text{m} / \text{N}$	$\pm 13 \mu\text{m} / ^\circ\text{C}$
Tip translation	$\pm 5 \text{ mm} / \text{N}$	$\pm 240 \mu\text{m} / ^\circ\text{C}$
Tip Twist in Torsion	$\pm 82 \text{ arcsec} / \text{Nm}$	$\pm 5 \text{ arcmin} / ^\circ\text{C}$
Tip Rotation in Bending	$\pm 25 \text{ arcsec} / \text{N}$	$\pm 3 \text{ arcsec} / ^\circ\text{C}$

The thermal conditions in space can be determined from known data. Based on the spectral distribution of the sun’s radiation, it has been shown that the sun emits radiation as if it were a black body at 5762K [Incropera and DeWitt, 2000]. The large space structures under consideration would be built in the low earth orbit (LEO) or the geo-synchronous earth orbit (GEO), which are 200 km and 36000 km, respectively, from the earth’s surface. Taking into account the diameter of the sun (1.39×10^9 m) and earth (1.28×10^7 m) and the distance between the earth and the sun (1.5×10^{11} m), the amount of solar radiation incident at that location is found out to be 1353 W per square meter of area. The surrounding temperature in space is taken to be 3K to account for cosmic microwave radiation.

A simple 2-dimensional beam element of dimensions 200 m x 1 m was analyzed using ideal heat transfer equations as well as the FEM software ADINA. The beam was modeled as a 2-D solid conduction element with a distributed heat flux on one side combined with radiative heat transfer from the top and bottom sides (Figure 2.5).

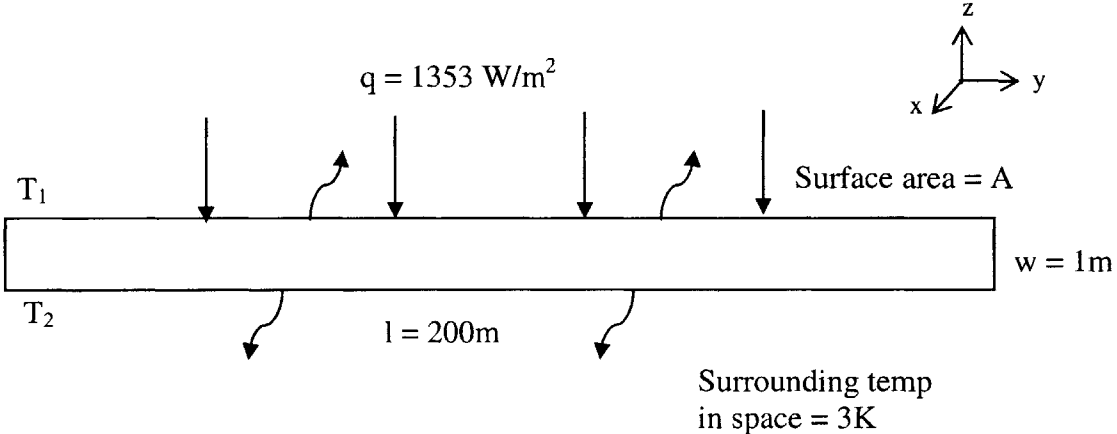


Figure 2.5: Heat transfer in a semi-infinite beam

The heat transfer equations for this system can be written as:

$$\begin{aligned}
 qA &= Ak \left(\frac{T_1 - T_2}{w} \right) + \sigma A \varepsilon (T_1^4 - T_s^4) \\
 Ak \left(\frac{T_1 - T_2}{w} \right) &= \sigma A \varepsilon (T_2^4 - T_s^4)
 \end{aligned}
 \tag{2.1}$$

where, k is the thermal conductivity of the material, ε is the emissivity of the surface and σ is the Stefan-Boltzmann constant. For ADAM beam properties, the temperatures at the top and bottom surfaces with respect to the sun were found to be 580 K and 250 K, respectively. Analytical results for the 2-D case compared well with the numerical results from finite element simulations. The temperature distribution across the beam was then used to perform a stress analysis to determine the thermal deformation of the beam. The numerical analysis was extended to the 3-D case in which there was radiative heat transfer from all four sides (Figure 2.6). See Table 2.2 for some sample deformation numbers for structures of different shapes.

The simple beam model was used to carry out simulations on different LSS shapes starting from a triangular truss (Figure 2.7) to a much larger truss. Results for a triangular truss have been illustrated below. Each side of the triangle was taken to be 200 m in length. Based on the beam material properties and the temperature conditions in space, maximum deformation of approximately 1 m was observed in the triangular truss. Deformation of this magnitude is quite significant and ignoring it during the assembly process may cause catastrophic failure in a space mission.

It was observed that while the deformation in the out-of-plane direction is significant, the in-plane deformation is 2-3 orders of magnitude smaller. This is due to the high stiffness of the truss in the in-plane direction and extreme flexibility in the out-of-plane direction. The deformation is also compounded for a larger truss structure.

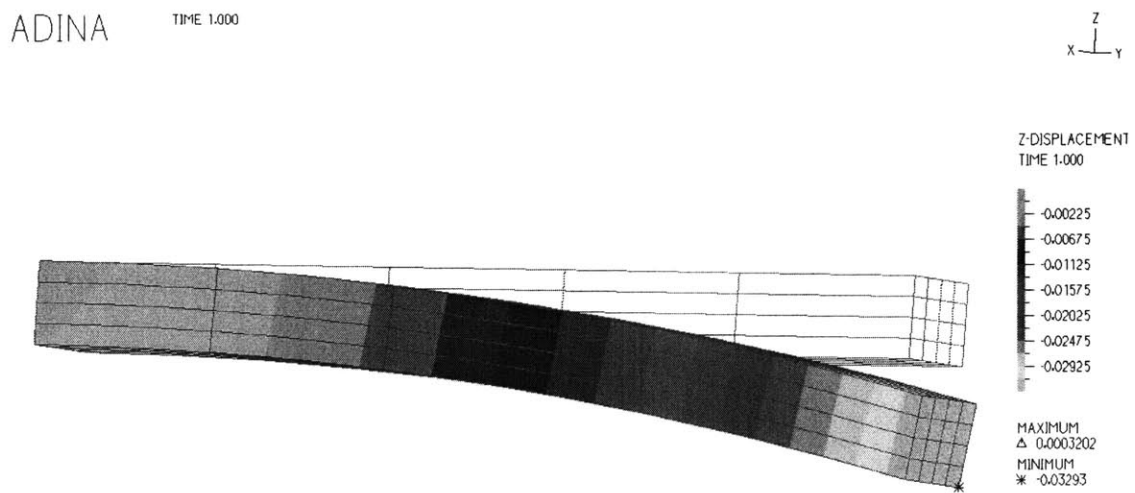
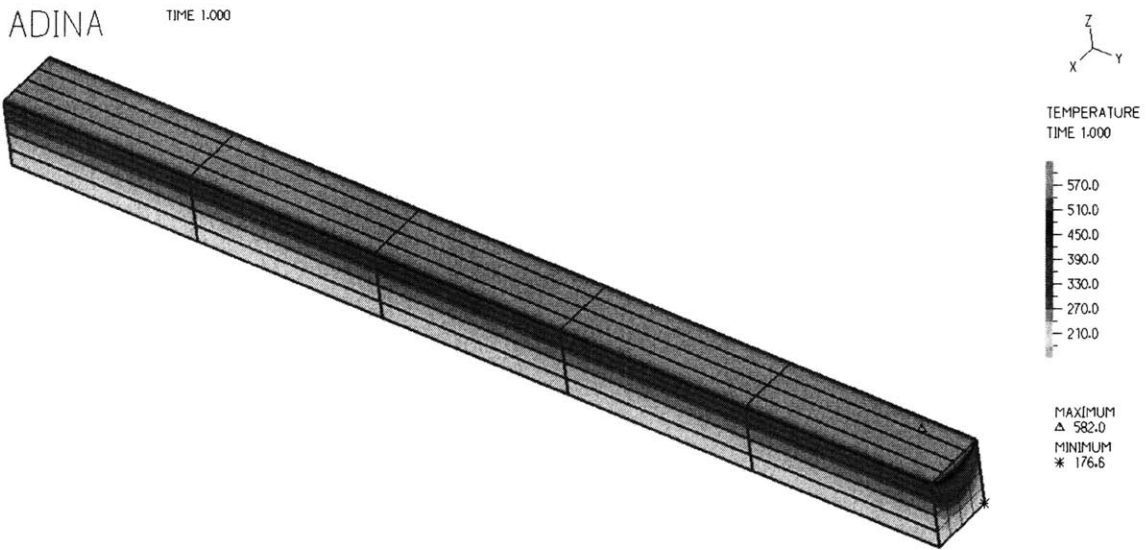
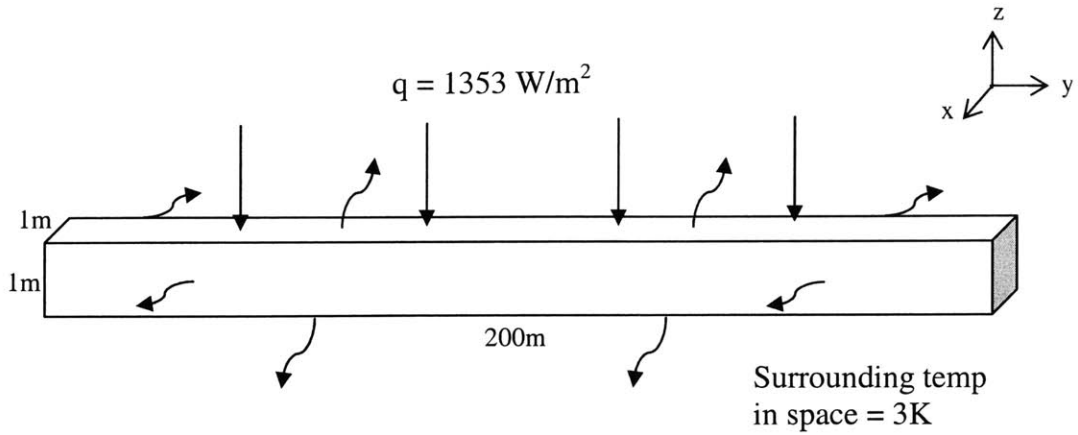


Figure 2.6: Simulating the thermal loads on a 3-D element (axes not to scale)

To analyze a realistic assembly process, it is necessary to develop a model for the thermally warped base truss having dimensions of about 2 km x 2 km and made up of these smaller triangular elements. This is much larger than the sizes considered above and creating a 3-D thermal model is computationally very intensive. However, once the thermal deformation is known, the mechanics of the structure can be modeled using just a 2-D planar model. This property has been exploited using MATLAB and ADINA and a finite element model of the thermally deformed base truss has been created. See Appendix A for details about the modeling. For a structure of this size, the maximum deformation was observed to be approximately 120 m.

Thermal analysis has been carried out under the assumption that solar flux on the structure is constant. Orbital motion of the structures in and out of the earth's umbra in LEO would violate that assumption and impart additional thermal effects. There would also be thermal effects due to radiation from the earth. These effects may not be significant in high altitude orbits like GEO [Malla et al., 1988]. Further analysis is required to study the effects of changing heat flux incident on the system.

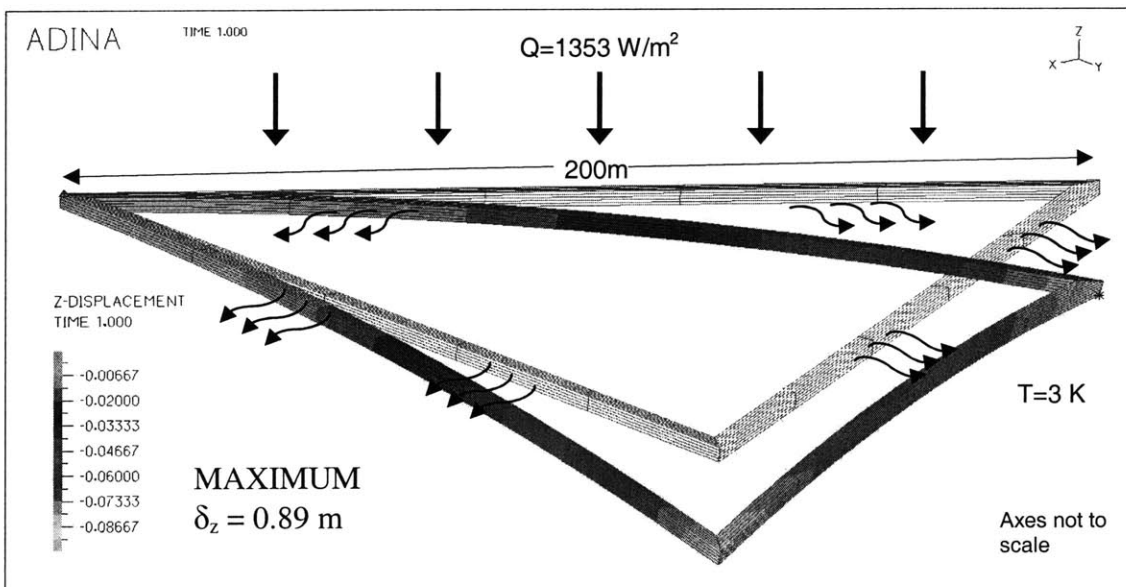


Figure 2.7: Thermal deformation of a triangular structure in space

2.3.2 Vibration Analysis

The large space structure finite element model described in the previous section can be used to perform vibration analysis. This is necessary to determine the nature of vibrations that may be induced by contact with robots. A finite element model of the LSS was set up in ADINA and the natural frequencies and mode shapes were determined (Figure 2.8). For free floating structures in space, the vibrations set up by an impulse were found to have periods of about 10-15 hours. Any unbalanced force applied to the structure may cause large displacements which may not damp out quickly. Knowledge of the structure mode shapes is important to prevent their excitation and thus prevent unwanted vibrations. This information will also impact assembly techniques where timing of the operation is important.

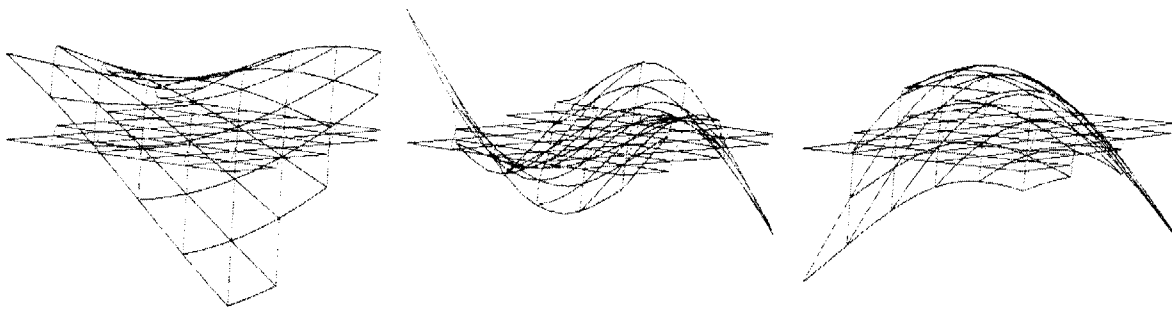
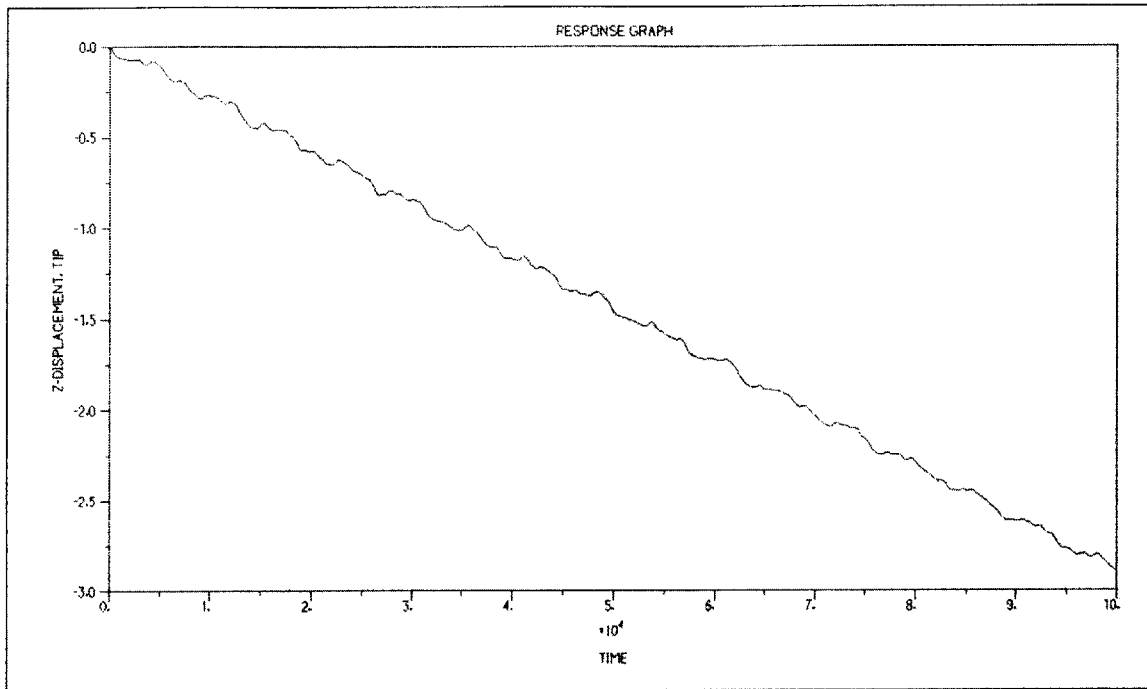


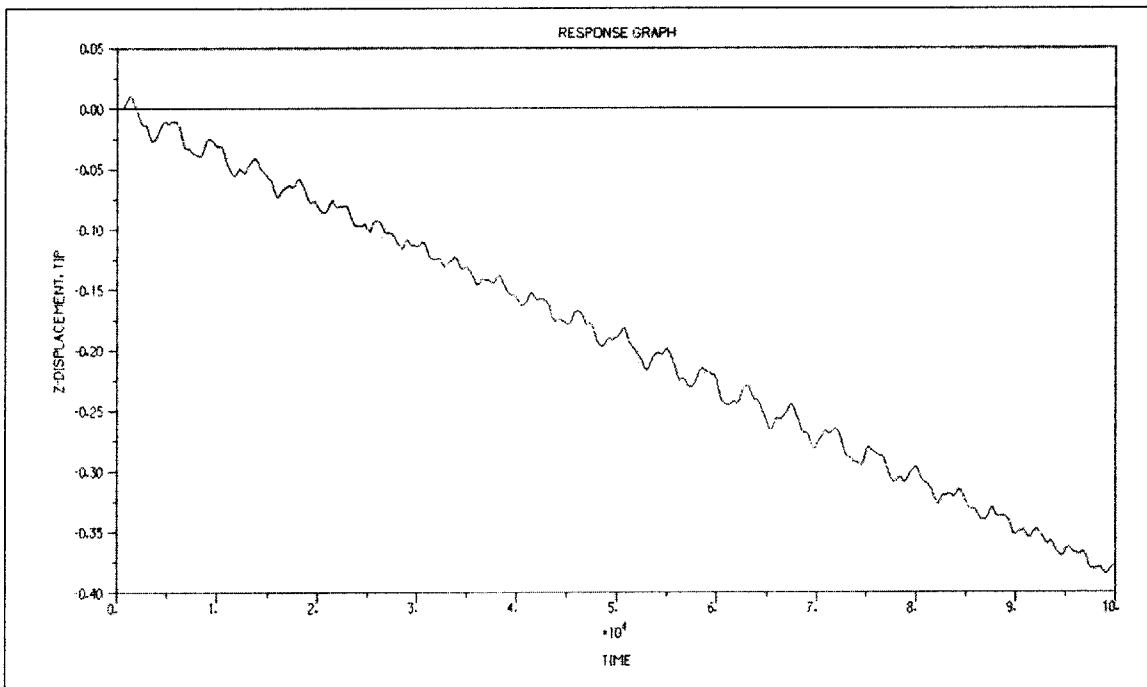
Figure 2.8: Various vibration modes of a typical large truss

Mode shape information is also used in the sensing process. The pose and dynamic parameters of a large space structure can be estimated in orbit using cooperative 3-D vision sensors and estimation algorithms like the one proposed by Lichter and Dubowsky [2003]. As seen in section 1.3, these techniques use Kalman filters to filter coarse estimates of the target's pose from vision sensor data and extract full dynamic state and inertial parameters of the target. The mode shapes would be useful in developing a dynamic model of the LSS to be fed to the Kalman filter.

Vibration analysis is also used to determine the impulse and step responses of the LSS to location specific loading. Approximate transfer functions for the system are extracted from this information and used in control analysis to determine damping coefficients that will minimize vibration. Thus approximate system dynamic models can be created. The global displacement of nodes in the base truss due to an impulse has been shown in Figure 2.9. Low frequency vibrations with time periods of several hours that will be set up in the structure can be observed in the displacement pattern.



(a) Displacement of a corner node



(b) Displacement of the center node

Figure 2.9: LSS impulse response

2.4 Assembly Methods

The previous section described causes for dimensional mismatch in large space structures that may adversely affect the assembly process due to thermal deformation and vibrations. Other factors like manufacturing tolerances in the lengths of the beams and joint precision characteristics will also impact the assembly process. This section looks at developing methods for compensation of these dimensional errors.

A typical large space structure assembly scenario would involve the joining of a small sub-structure (of the order of 100-200m in dimension) to a much larger structure (of the order of a few kilometers in dimension). One way to perform assembly in the wake of dimensional mismatch would be to use free-floating robotic systems to bend the warped structures into place. The large space structures under consideration are inherently flexible due to their thin plate-like nature and do not require huge forces for deformation. Hence, the assembly process involves grasping connection points on the mating trusses with free-floating manipulators and forcing them together by the combined deformation of both trusses. The following tasks need to be carried out for the assembly process:

- Estimation of the magnitude of mismatch – This can be obtained from the previous analysis of thermal deformation
- Estimation of forces required
- Development of sensing techniques to determine actual locations of mating points

2.4.1 Cooperative Robots

It would be impractical to use astronauts performing extra-vehicular activity (EVA) to carry out the assembly process across distances ranging in kilometers. Using multiple robots is a viable solution to this problem. The various tasks involved in the assembly process thus would be carried out by teams of robots operating cooperatively. Proposed solutions would take into account this distributed sensing and actuation. Multiple robots would estimate the structure's dimensional mismatch using their vision

sensors and perform deformation using their actuators. The robots would perform the tasks subject to the following constraints:

- Shape/size of the structures
- Power consumption
- Safety of approach paths
- Communication delays between robots
- Sensing delays
- Errors
- Thruster plume impingement

2.4.2 Forced Assembly by Robot Manipulation

To assemble the warped structures, sufficient forces must be applied at the joints to cause the entire structure to deform temporarily to the desired shape (Figure 2.10). The forces required to deform some thermally warped structural shapes can be determined using the finite element model of LSS developed in section 2.3.1. These have been listed for different LSS shapes in Table 2.2. Note that the analysis for each truss shape has been carried out keeping one joint fixed and deformation has been measured relative to this fixed joint.

Cooperative free flying robots would sense the position error and fit the mating objects into place. However, a variety of factors may make it impossible for direct application of force at the point of deformation, such as plume impingement, awkward and unwieldy shape of the structure or the robot, errors in attitude of the robot with respect to the structure and hence errors in the line of application of the forces, etc. This implies that robots would have to apply forces at some other suitable location and remotely cause deformation at the mating point. The task now is to determine the magnitude and location of these forces.

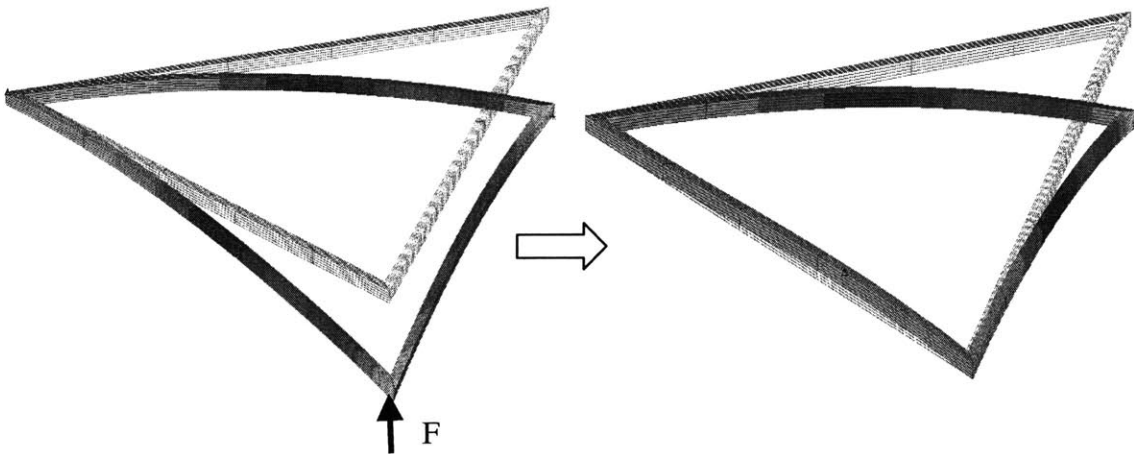
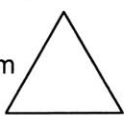
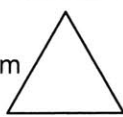
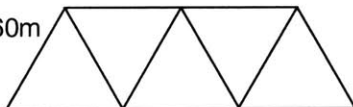


Figure 2.10: Forced deformation to desired shape (exaggerated for effect)

Table 2.2: Deformation and forces required for assembly for different truss shapes

Truss shape (Each member c/s – 1m x 1m)	Maximum Deformation (under thermal loading in space)	Force Required
60m _____	10 cm	12 N
200m _____	89 cm	3.5 N
60m 	9 cm	12.5 N
200m 	88 cm	3.6 N
60m 	77 cm	5.8 N
60m 	78 cm	6 N

This problem can be solved by individually analyzing the deformations caused in the structure due to each candidate force. The points of application as well as force directions are chosen to take into account all the constraints. A linear system model is assumed in which the bending of the structure can be represented by a transformation matrix T . This matrix relates the effect of forces applied at some specified points to deformation that is caused at certain other points of interest. The linear assumption is valid as the deformations being considered (about 1 – 10 m) are much smaller compared to the size of the truss (100 – 1000 m). Mathematically, this can be stated as follows:

$$T \vec{F} = \vec{\Delta x} \quad (2.2)$$

For example, in Figure 2.11, the input points at which forces are applied are 1, 3 and 5. The output parameters of interest are the x displacements of the same points. Thus there are 3 input parameters and 3 output parameters. To determine the transformation matrix, forces are individually applied to the finite element model of the truss in ADINA. The effect of each force at the points of interest will give columns of T . Once T is determined, its inverse can be computed to predict the forces required to carry out some required deformation Δx , or

$$\vec{F} = T^{-1} \vec{\Delta x} \quad (2.3)$$

This technique was verified by loading the truss finite element model with the predicted forces. It was found that the truss bent back into the desired shape (see Figure 2.12).

The transformation matrix described for the problem above is a square matrix whose inverse can be found easily. In general, a small number of robots can be used to carry out the required deformation at a large number of points leading to a distributed actuation network. Here a small force vector controls a relatively large displacement vector and the transformation matrix is not-square. For example, consider the case in Figure 2.11 where x-displacements of points 1, 2, 3, 4 and 5 are taken to be the output variables. The transformation matrix has a dimension of 5 x 3. This problem can be solved by using the matrix pseudo-inverse.

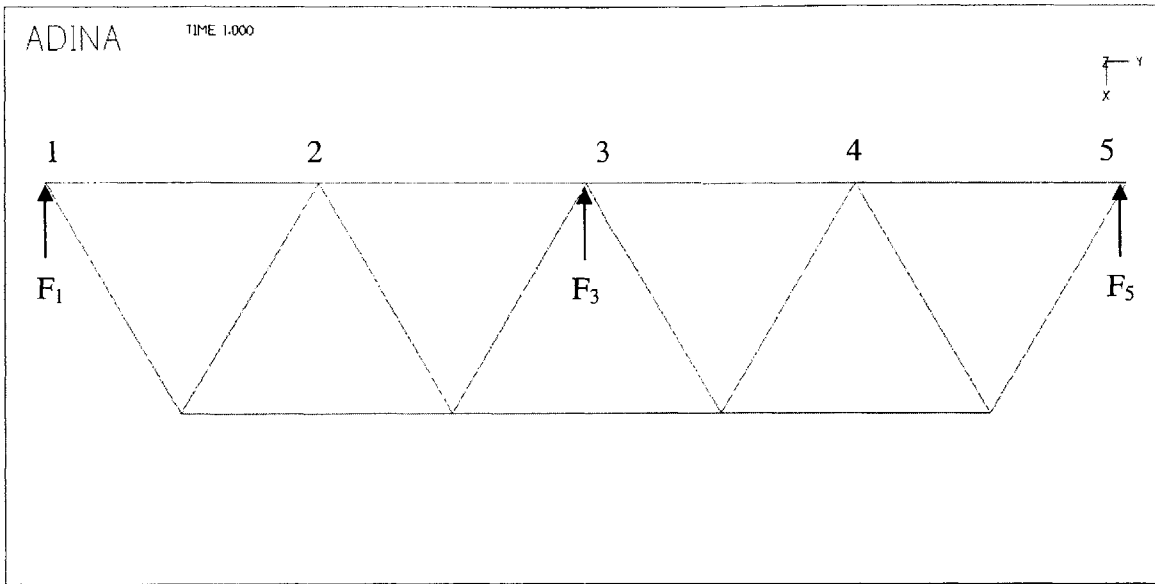


Figure 2.11: Force analysis setup in ADINA

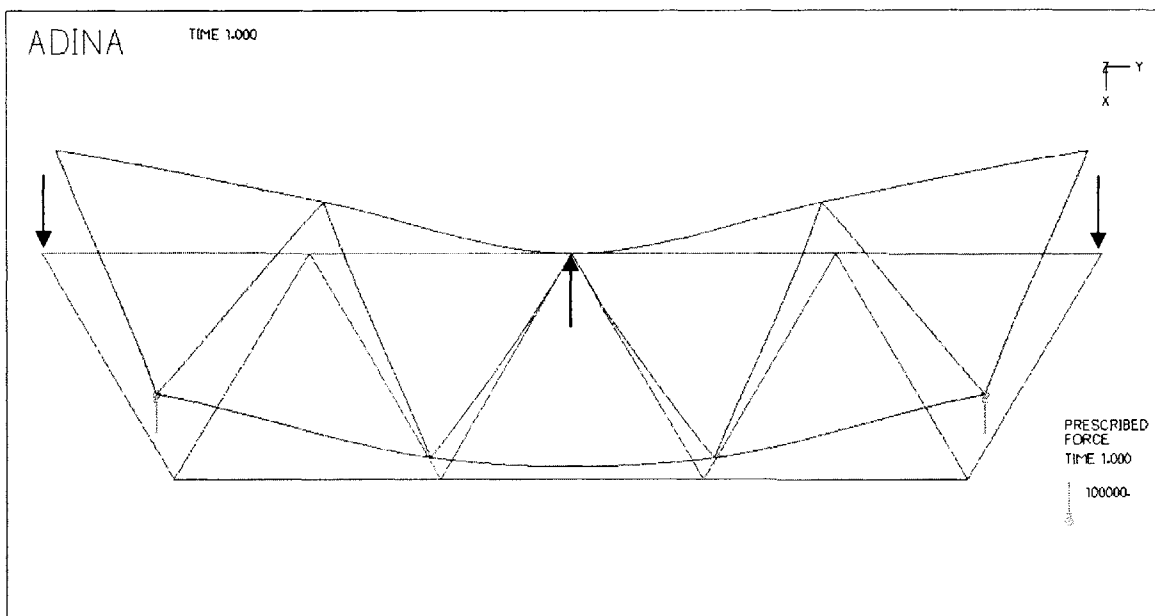


Figure 2.12: Large space truss bent back into shape under application of forces

The pseudo inverse of this matrix can be computed as:

$$\mathbf{T}^\# = \mathbf{T}^T [\mathbf{T} \mathbf{T}^T]^{-1} \quad (2.4)$$

The force vector can therefore be computed as:

$$\therefore \vec{F} = \mathbf{T}^\# \vec{\Delta x} \quad (2.5)$$

The results obtained have been verified by plugging back into the ADINA finite element model to determine the actual shape. This conformed to the desired shape of the truss as shown in Figure 2.13.

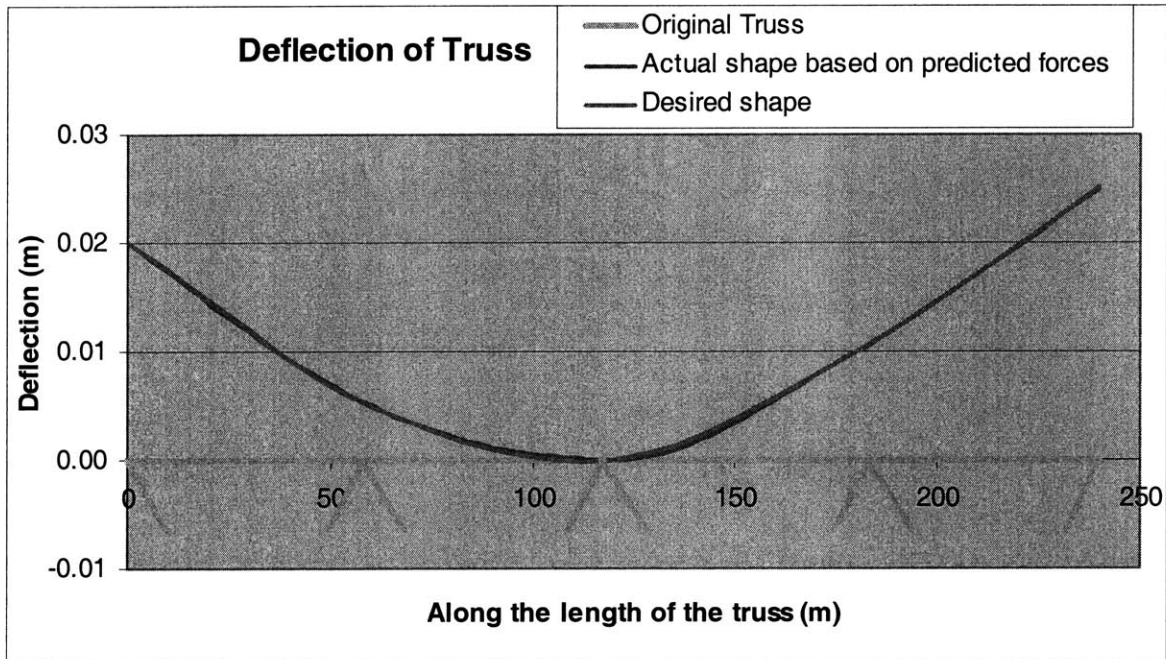


Figure 2.13: Comparison of actual shape of the truss based on predicted forces with the desired shape

2.4.3 Thrusters for Assembly

Robot manipulators are extremely versatile and can be used to solve assembly problems due to deformation of space trusses. These solutions involve grasping of the mating structures by the manipulators and forcing them into place. This strategy, however, will fail in situations where the deformation is large enough to be beyond the reach of the manipulators. In such scenarios, thrusters will have to be used as actuators due to their ability to apply forces independent of the assembly system. Some differences between thrusters and manipulators are:

- Manipulator forces are less expensive as electrical energy supplied to the motors can be stored in batteries and possibly recharged from solar power. Thrusters are costly due to the weight of the jet fuel. Also, thrusters have to be recharged for which additional effort and setup is required.
- Thrusters have less precise actuation characteristics than robot manipulators [Wertz, 1985]. Robot manipulator control methodologies are well-developed and vastly studied as compared to thruster control methods (like bang-bang control). This makes manipulators more dexterous and versatile. Also, control of the force application direction in thrusters is not as accurate.
- There is a safety issue involved in the use of thrusters due to the risk of plume impingement with the LSS.
- Manipulators can only be used at contact points that are within their reach whereas thrusters may be used anywhere.
- Thruster applications must be followed by suitable manipulator grasp so as to maintain the structure in deformed shape and perform assembly.

Figure 2.14 shows a representative thrust profile for a gas-jet system. Some typical delays and inaccuracies associated with the thruster control system are highlighted [Wertz, 1985]. Intervals t_0-t_1 and t_3-t_4 are due to electrical and mechanical delays and to the time required by the propellant to flow from the valves to the thrusters. Intervals t_1-t_2 and t_4-t_5 are the rise and fall times for the propellant to establish a steady-state flow. In addition, steady-state thrust is not exactly constant due to errors and noise associated with it.

All these drawbacks make thrusters an unattractive proposition for use in the assembly process as compared to manipulators. However, as discussed above, thrusters must be used in situations where use of robot manipulators is physically impossible.

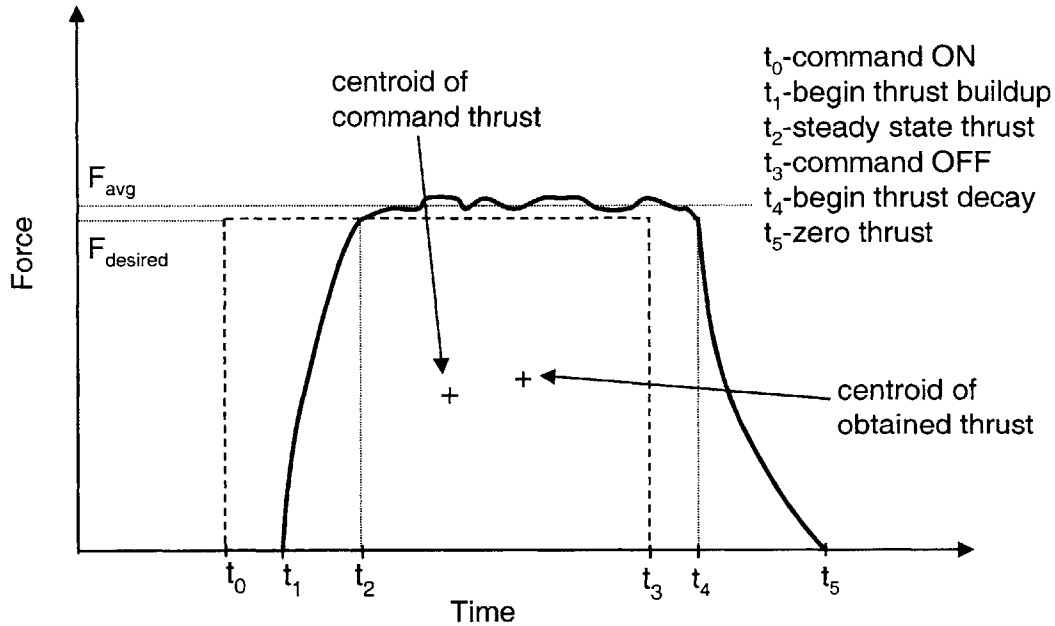


Figure 2.14: General Thrust Profile for Gas-Jet Control Systems

2.5 Summary

This chapter developed a methodology for large space structure assembly. The assumptions made as a basis for this work were laid out. The static and dynamic effects on a typical large space structure were analyzed. Thermal and vibration analysis was carried out using finite element models to estimate deformation in the space structures. The assembly problem was discussed and forced assembly methods using cooperative robots were developed.

3.1 Optimal Assembly Planning

A large space structure assembly scenario involves the use of multiple robots working cooperatively to join truss structures while overcoming dimensional mismatch caused by thermal, vibration and other effects. Robots would apply forces at multiple connection points to force the mating structures into place using an efficient assembly strategy while ensuring the stability and safety of the system. This requires an assembly planning method and algorithms for execution. These techniques are developed below for various assembly scenarios.

3.1.1 Numerical Optimization Methods

The forced assembly methods developed in section 2.4 can be used to determine the magnitude of forces to be applied to a truss to achieve a desired deformation. However, there may be many possible combinations of forces that may achieve the same result, possibly using fewer resources, implying that the solution obtained may not necessarily be optimal with respect to resource consumption. In this section, a method is described that optimizes the force application for the number of robots while taking into account a set of constraints.

Optimal Force Application

Robots used in the space structure assembly process would have limited resources at their disposal. In particular, their force capabilities would typically be restricted due to the limitations of the actuators like manipulators or thrusters. As seen in Table 2.2, maximum forces would be of the order of 20-30N. In case of thrusters, the force magnitude would directly affect the fuel consumption. The task, therefore, is to determine the optimal number and location of forces that would bend the truss to the desired shape and use the least magnitude of forces. The optimization problem can be formulated as follows:

$$\begin{aligned}
 & \min && \text{Cost Function } CF = w_1 e^{norm} + w_2 \sum F_n^{norm} \\
 & \text{subject to} && (i) \text{ Force locations restricted to be on the truss} \\
 & && (ii) \text{ Force magnitudes restricted to be with the} && (3.1) \\
 & && \text{maximum limits} \\
 & && (iii) \text{ Bending error depends on the elastic} \\
 & && \text{deformation of the truss}
 \end{aligned}$$

where,

CF = cost function value

w_1 = weight of normalized error in the cost function

e^{norm} = normalized mean squared error in deformation of the structure due to applied forces as compared to the desired shape

w_2 = weight of force magnitudes in the cost function

$\sum F_n^{norm}$ = Sum of normalized forces. The normalization is performed by using an exponential utility curve which penalizes heavily for large forces (Figure 3.1). This can be viewed as a function that minimizes energy consumption of the robots if, for example, the forces are being applied by thrusters.

The sequence of steps in the force optimization algorithm is shown in Figure 3.2. An initial guess of the optimal solution is made to initialize the optimization. The cost function is highly non-linear and hence the algorithm may converge to local minima leading to a sub-optimal solution. A better solution can be obtained by heuristically choosing the initial guesses for forces and locations so that they are close to the global optimum and convergence is likely. For example, in the case of a simple beam clamped

at one end, a force applied at the tip will cause maximum deformation. Hence, the tip location can be chosen as the initial guess.

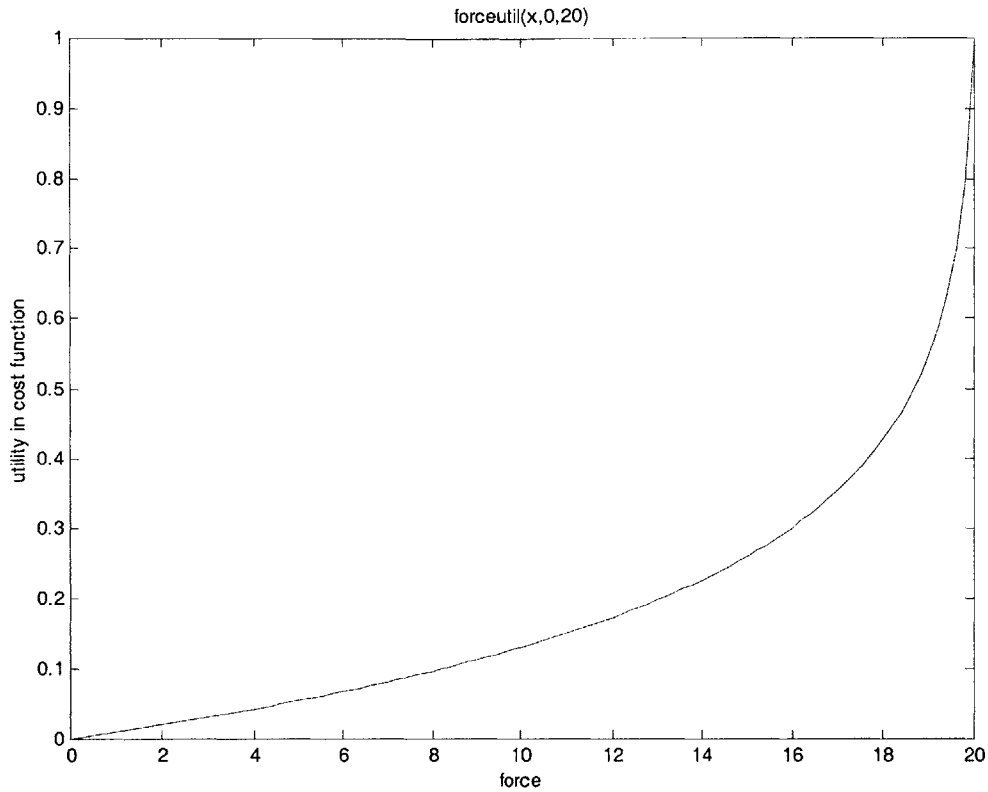


Figure 3.1: Utility of applying a force in the cost function

Another approach would be to choose initial variables randomly within the allowable range and determine the optimal solution for multiple trials. If the number of iterations is large enough (typically about 10,000), the entire sample space would be scanned for local minima. The best solution corresponds to the minimum of all these local minima.

An important thing to note here is that the weights w_1 and w_2 described above need to be carefully chosen depending on whether the shape error in bending or the force vector is the critical factor.

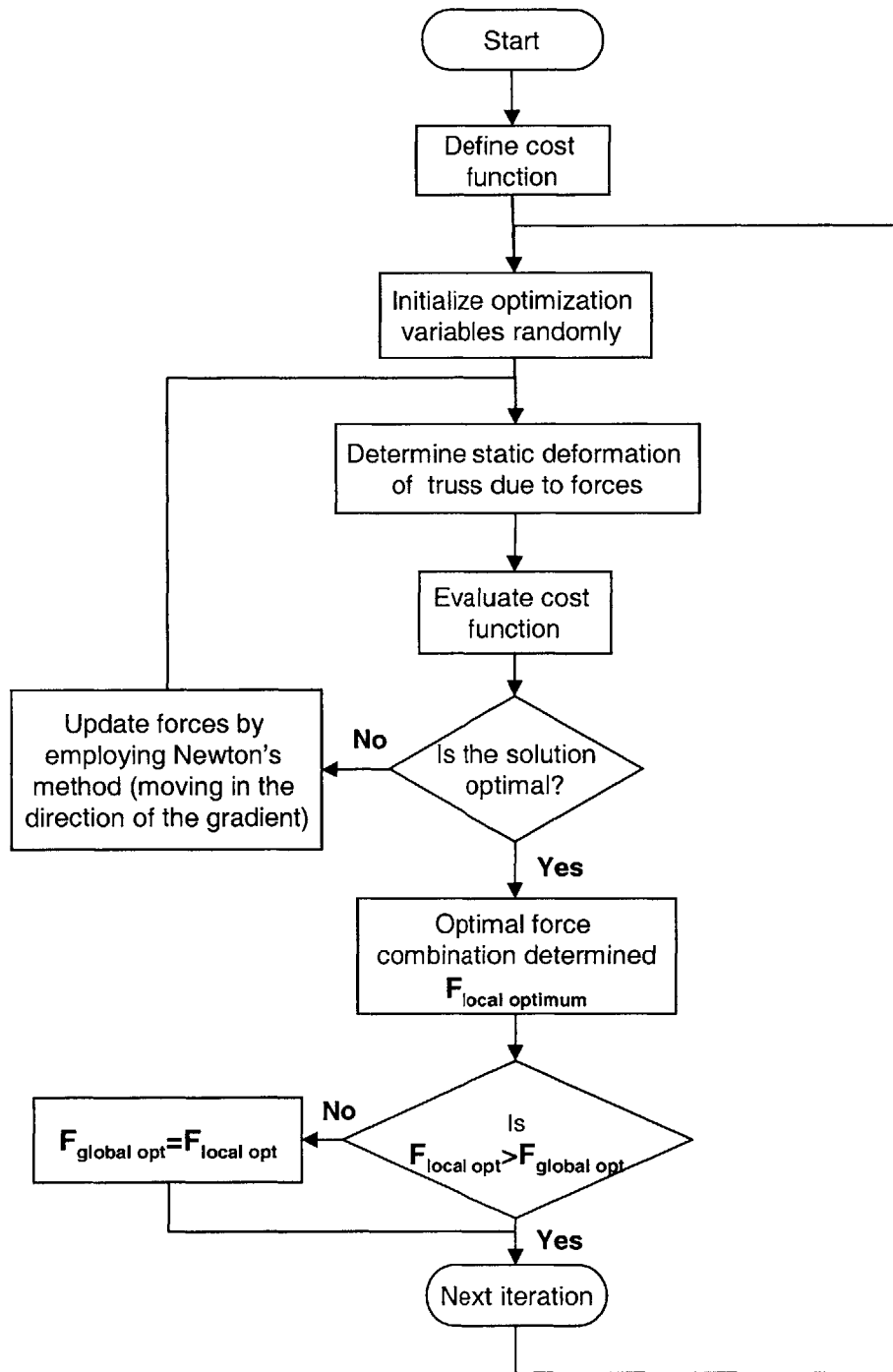


Figure 3.2: Force optimization algorithm

The above force optimization algorithm was applied to the case of simple beam bending (Figure 3.3). Static deformation due to applied forces was computed from the finite element model. The error distribution for a single force with varying magnitudes and locations has been plotted in Figure 3.4. It can be seen that local minima for error exist at points along an arc. In many instances, the optimization routine converged at some of these points depending on the initialization of the variables. Multiple iterations with random initial guesses finally converged to the global minimum for sufficiently large number of iterations. As expected, force applied at the tip of the beam is the optimal solution to the problem. The required force magnitude was 3.3 N.

The required forces for deformation were also computed from an analytical model of the beam. This is used to check the validity of the finite element analysis. An optimality condition was similarly set up and subject to the constraints of minimizing the RMS error as well as the magnitudes of the forces required. The results for both cases have been shown in Figure 3.4 and are in close agreement.

To study the effect of using multiple robots, the above analysis was carried out with multiple forces. The minimum shape error that can be achieved for a given number of robots was determined. As seen from Figure 3.5 there was almost an exponential reduction in the error. Two robots were more than sufficient to bring the shape error within desired limits (0.02 m according to the joint tolerance assumption).

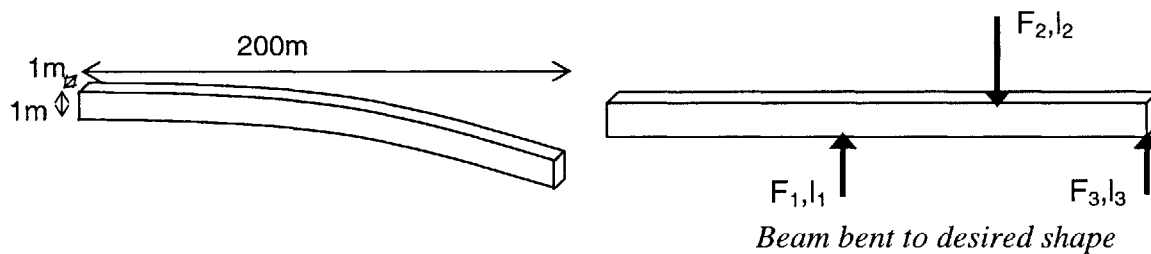


Figure 3.3: Optimal bending of a beam element

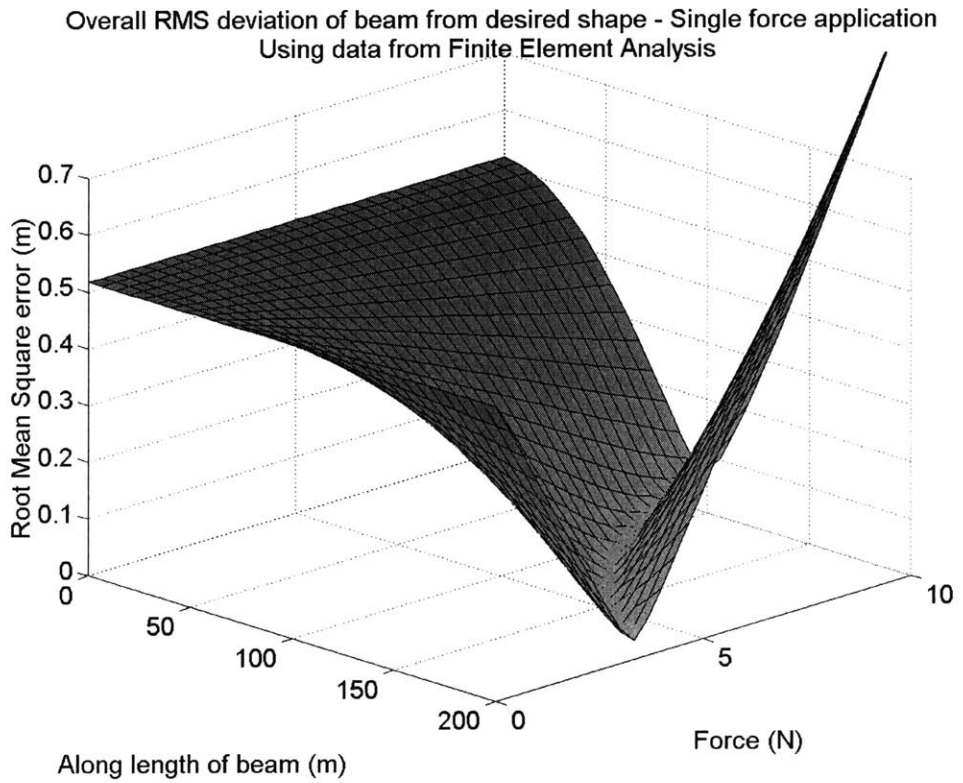
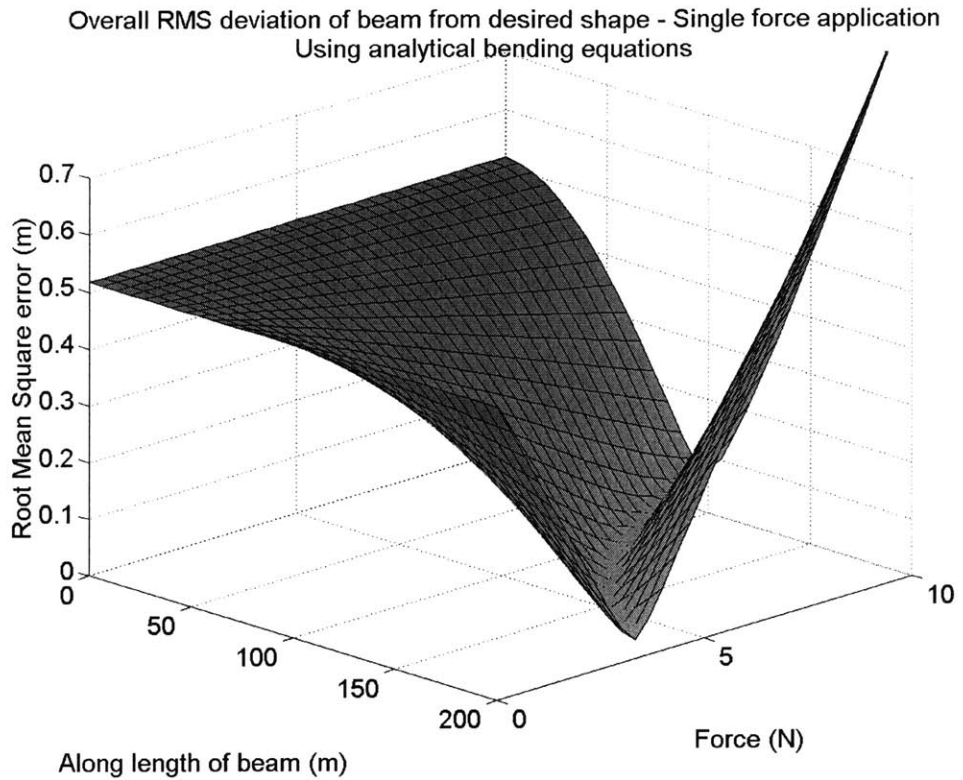


Figure 3.4: 3D plot of error in bending a beam vs force magnitude and location. Beam bending is computed analytically as well as using a finite element model

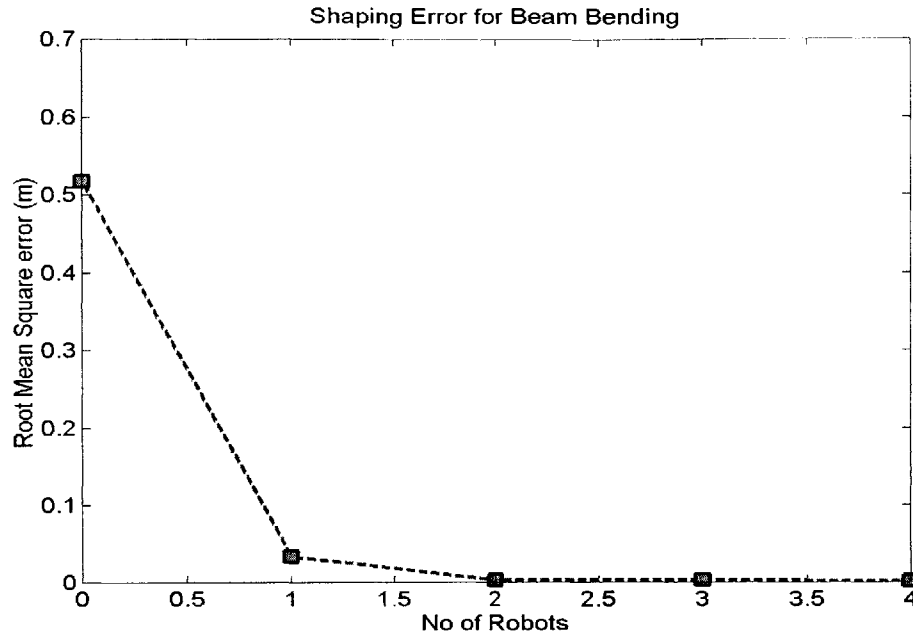


Figure 3.5: Shape error variation with number of robots

3.1.2 GA-based Optimal Approach to Assembly

The assembly scenario would not only involve the optimization of forces (magnitude and location) but also the number of robots used. Given the huge number of variables involved, a simple force optimization algorithm will not be adequate to yield the desired results. A genetic algorithm (GA) based assembly planner has been developed that will synthesize all the inputs and resources and develop the most cost-effective assembly plan. The following features have been incorporated into the planner:

- Deformations of the triangular truss are pre-computed for certain force locations and magnitudes using an accurate finite element model from ADINA. The deformation required by the GA for any given force location and magnitude is obtained by interpolation.
- Penalty is imposed in the cost function for resources used, including number of robots, magnitudes of forces applied, etc. Some resources may be more expensive than the others.
- Penalty is imposed if there are mismatch errors at the end of an assembly operation based on the developed assembly plan.

- Robots may use two kinds of actuators – manipulator arms or thrusters. The differences between them are discussed in detail in the subsequent sections.
- Connection between trusses is assumed to be made when the distance between grasping points is within grasp tolerance.

Implementation of the GA based Assembly Planner

The planner has the following control variables:

- Number of robots
- Number of assembly steps – Robots would apply forces during an assembly step and make connections. After each step, robots would reorganize themselves and apply forces again during the next step.
- Location of each robot at each step
- Magnitude of forces applied by each robot at each time step
- Force direction and application type – e.g. thrusters or manipulators

The objective function for the GA has the following parameters with suitable normalized weighting factors associated with them:

- Difference between deformed shape and desired shape – This is the measure of success of the assembly operation
- Magnitude of forces exerted by the robots – This is a measure of energy consumption
- Type of forces – This is a measure of impact on robot life
- Number of robots
- Distance traveled by the robots – This is a measure of energy consumption

Validation and Refinement

For validation purposes, the planner has been tested with simple scenarios where the solutions are 'obvious'. It is necessary to adjust the weights for different parameters in the objective function to suit the particular task at hand. For example, a critical assembly task may put a premium on dimensional mismatch at the cost of additional robots being employed for the task. As a result the weighting factor associated with the number of robots will be low while that with the dimensional error will be high.

Some results have been obtained for the case of assembly of a triangular truss (200m side) by connection at the 3 corners. Figure 3.6 shows possible node locations and numbers for force application. The initial deformation at the two remaining corners after the first joint connection has been made is 2 m.

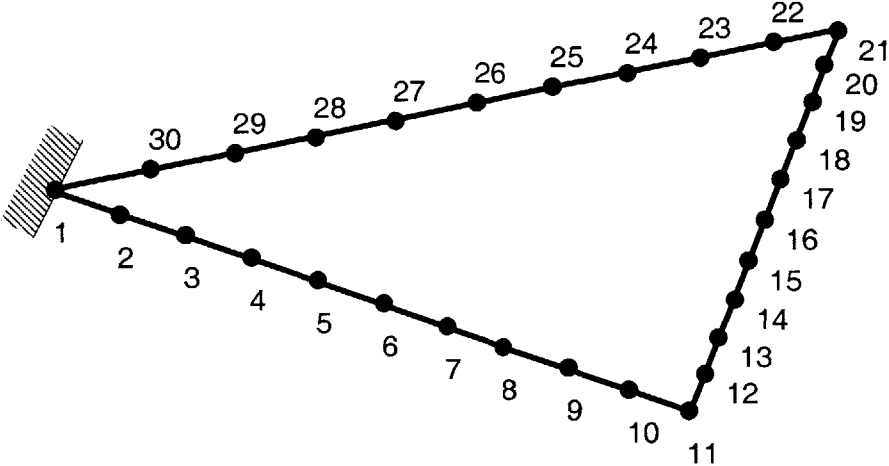


Figure 3.6: Node locations for force application on triangular truss

(i) Case 1: Here the maximum force is 20 N, and thrusters (T) and manipulators (M), are assumed to be equally expensive

Assembly plan:

```
Number of Robots = 1
Number of Steps = 1
STEP 1
Force (N) : 14.839 N
Force Type:      T
Location  :      16
```

The planner recommends the use of one thruster applied at the mid-point of the truss with respect to the fixed end

(ii) Case 2: Here the maximum force is 10 N, and thrusters (T) and manipulators (M) , are assumed to be equally expensive

Assembly plan:

```
Number of Robots = 2
Number of Steps = 1
STEP 1
Force (N) : 9.0323 5.1613
Force Type:      T      T
Location  :      19      11
```

The force limit in this case forces the planner to use 2 robots for the assembly task as a single robot cannot apply the required 14.84 N force.

(iii) Case 3: Here the maximum force is 20 N, and thrusters (T) are assumed to be much more expensive than manipulators (M)

Assembly plan:

```
Number of Robots = 2
Number of Steps = 1
STEP 1
Force (N) : 9.0323 5.1613
Force Type:      M      M
Location  :      19      11
```

In the case, the planner chooses to use the cheaper manipulators as opposed to the expensive thrusters. Since manipulators cannot be used at location 16 because there is

no underlying structure to grab on to, the planner uses two robots at locations 19 and 11 instead of one at location 16.

(iv) Case 4: Here the maximum force is 20 N, and the use of each robot is extremely expensive. Also, thrusters (T) are assumed to be much more expensive than manipulators (M).

Assembly plan:

Number of Robots = 1

Number of Steps = 2

STEP 1

Force (N) : 9.0323

Force Type: M

Location : 19

STEP 2

Force (N) : 5.1613

Force Type: M

Location : 11

The planner uses only one robot with manipulators in two steps thereby avoiding the cost of one robot.

The GA based planner has been developed to analyze some representative scenarios that will be discussed in subsequent sections. It is by no means a complete tool to analyze general assembly scenarios, nor does it exhaustively deal with all variables that may be involved in the assembly process. The planner will have to be modified to accommodate new scenarios.

3.1.3 Optimal Robot Pose

Robots will be required to apply controlled forces to a structure during an assembly process. Consider an assembly scenario in which a robot grasps the mating ends of the base truss and the triangular truss that are separated by some distance due to deformation. Robot features including link lengths, joint angle limits and maximum torque capabilities are known. The assembly task involves application of forces that will bend the trusses into place. A robot with powerful motors will be able to apply large forces from its manipulators and deal with a wide variety of such assembly tasks. However, for given torque capabilities, the maximum force output from the manipulators will vary depending on the geometric configuration of the robot. It is desired to obtain the configuration that will maximize force output. One method of solving the problem is to determine the best feasible path using the force workspace (FW) of the robot [Madhani, 1997]. The FW maps system constraints like actuator torque limits and link lengths into a robot's joint configuration space to form constraint obstacles. A feasible path in the configuration-space can be obtained that does not violate these constraints. This path, however, may not necessarily be the optimal path that will give maximum force output.

The above problem can be formulated as an optimization problem as follows:

$$\begin{aligned}
 & \max && \text{Force } F \\
 & \text{subject to} && F = f(T_1, T_2, \dots, T_n, \theta_1, \theta_2, \dots, \theta_n, r) \\
 & && 0 < T_1, T_2, \dots, T_n < T_{\max} \\
 & && 0 < r < \text{maximum robot reach} \\
 & && \theta_{\min} < \theta_1, \theta_2, \dots, \theta_n < \theta_{\max}
 \end{aligned} \tag{3.2}$$

The function f is a relationship between F and the different variables involved that combine the kinematic and the force-torque equilibrium conditions. Appendix B has a complete solution for a robot with two single link arms (see Figure 3.7). Figure 3.8 shows the variation of force applied by the robot on the structure (y-axis) for varying joint angles (x-axis) and given values of a , r , L , θ_{\min} , θ_{\max} , T_{\max} . The curves represent increasing input torque T_1 from 0 to 10 Nm. As seen from the plot, maximum force output is obtained for the configuration: $\theta_1 = 45^\circ$ and $\theta_2 = 151^\circ$. It is interesting to note that the symmetric case is not necessarily the optimal one.

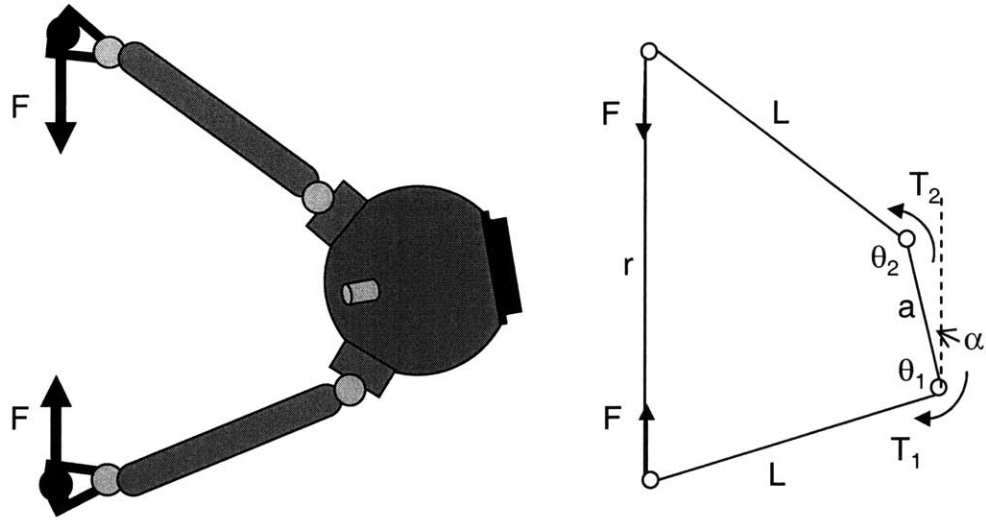


Figure 3.7: Determining the optimal robot pose for assembly

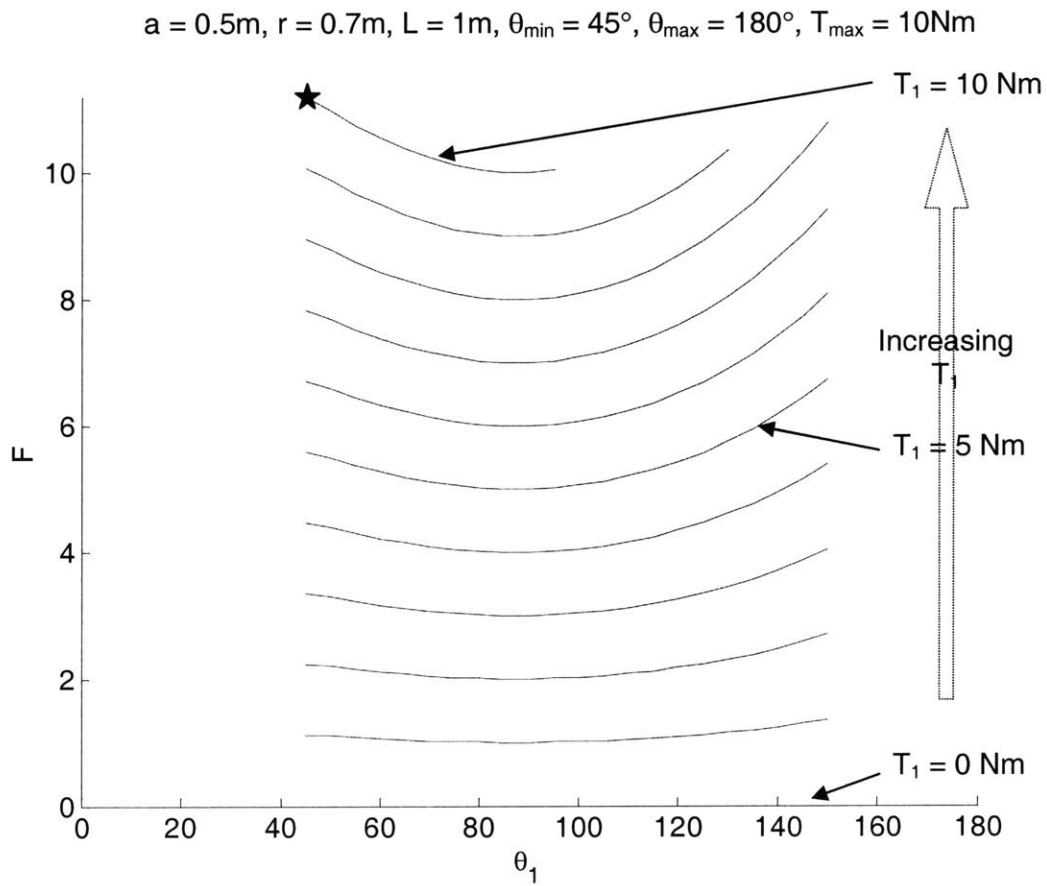


Figure 3.8: Optimal pose for maximum force output (plotted for different T_1)

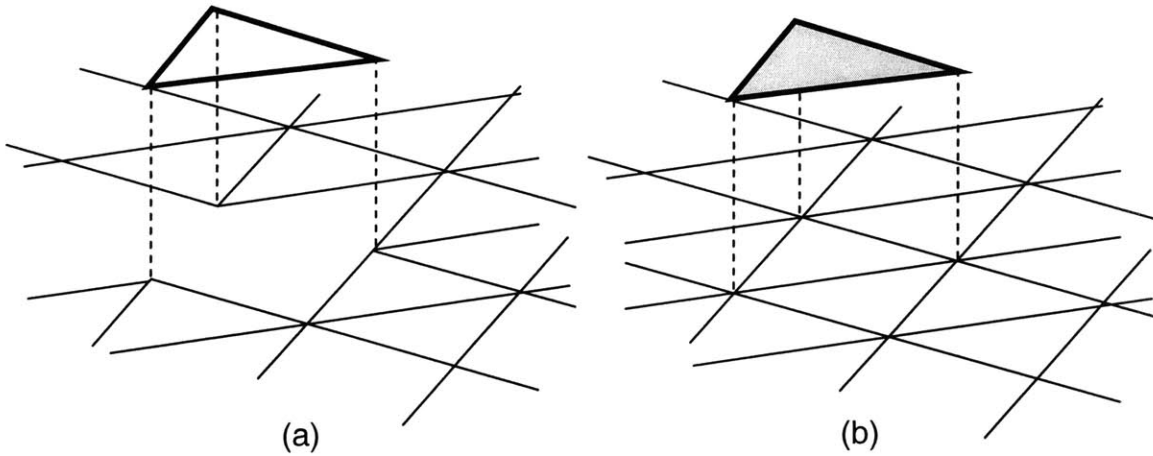
3.2 Inputs

The space solar power station (SSPS) described earlier is a representative large space structure. The construction of this LSS would involve assembly of huge reflecting mirrors, a secondary mirror/lens and power generation and transmission modules. The mirrors, for example, would involve truss construction in which smaller triangular trusses would be assembled onto a larger base truss (see Figure 2.2). When constructed, the entire truss would act as a huge mirror to reflect solar radiation to the power generation module. The assembly, therefore, could be of reflecting panels onto an existing framework or that of the framework itself. These tasks are inherently different and must be analyzed separately.

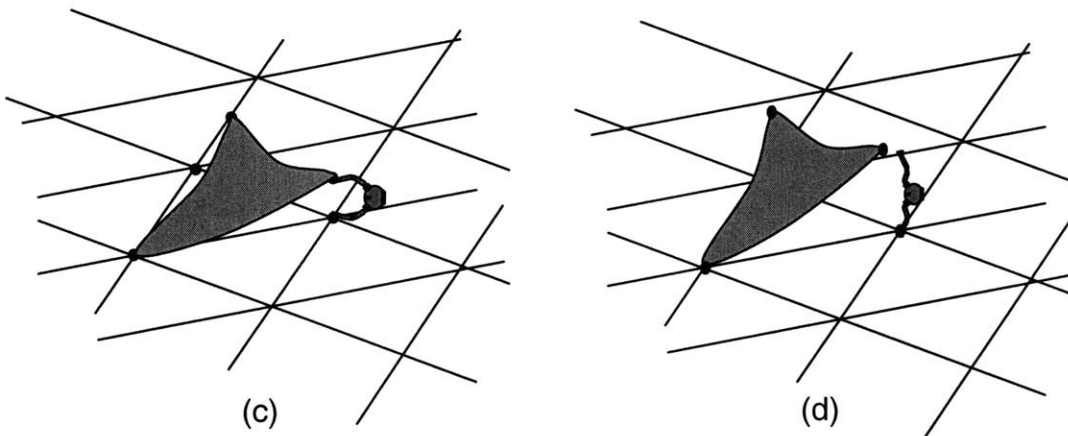
The methods mentioned in the previous section have been applied to several hypothetical but reasonable scenarios to study the assembly process. Reasonable assumptions have been made regarding various parameters involved in the assembly process and a detailed analysis has been carried out. The variable parameters in these scenarios are:

- Stiffness and mass of the base truss relative to that of the small truss
- Relative magnitude and direction of the deformation occurring in both trusses
- Robot actuator characteristics
- Joint tolerance requirements

The taxonomy of these assembly scenarios can be discussed based on the type of truss construction, whether the small truss goes into a hole or on to a frame, and the magnitude of deformation involved (whether it is within the reach of robot manipulators or beyond reach). This has been depicted in Figure 3.9. The latter condition determines the types of actuators used by the robots. Robot manipulators are usually less expensive to use than thrusters. As a result, there would be a class of assembly cases that could be carried out using only manipulators. These scenarios would involve deformation that is within the reach of the manipulators. From the robot model described earlier, a deformation of more than about 2-3 m is likely to be beyond the reach of the robot (depending on the force requirements and the robot workspace limitations). A detailed analysis of the robot force workspace is presented in subsequent sections.



Truss types – hole or frame



Deformation types – within reach or beyond reach of manipulators

Figure 3.9: Taxonomy of assembly scenarios

In this section, assembly scenarios were considered that involved small-scale deformations requiring only the use of robot manipulators. Section 3.3 deals with the analysis of some typical assembly scenarios involving large-scale deformations where robot manipulators may not be as useful.

3.3 Small Scale Deformation Scenarios

3.3.1 Single Connection Point

The problem considered here is the assembly of the basic truss framework. Hence, there is no underlying structure and connections need to be made at a single connection point per side of the small truss (See Figure 3.9 a & c). In addition:

- The base truss is assumed to be much stiffer than the small truss and also has a very large mass as compared to the small truss. Hence its bending or deformation due to forces or thermal loads can be neglected and it can be considered as being rigid and fixed. All deformation occurs in the small truss only
- Structure misalignment occurs only due to thermal loads in the out-of-plane direction. In-plane misalignment is negligible.
- The dimensional mismatch between the trusses is within the reach of the robot manipulators and the forces required for deformation are less than the maximum force that can be exerted by the manipulators.
- The joint tolerances are approximately 0.02m and hence connections can be made if the mating parts are brought to within this distance of each other [NASA ISS Program, 1997].

Assembly Plan

Three points on the small truss need to be connected to three corresponding points on the base truss. The first joint connection is unconstrained and can be connected without significant forces. As shown in the thermal analysis in section 2.3.1, a triangular shaped truss having sides 200m long warps due to thermal loads in space. A model of this triangular truss was created in ADINA and a thermal and structural analysis yielded a maximum out-of-plane deformation of 0.88 m at the corners of the truss. As a result, the second and third joint connections were not unconstrained. It was found that a force of 3.55 N had to be applied to bend the truss into place. This also caused a deformation at the third joint location. The total deformation at the third joint reduced to 0.73 m at this stage. A force of 5.12 N had to be applied to make the last connection in the assembly process. See Figure 3.10.

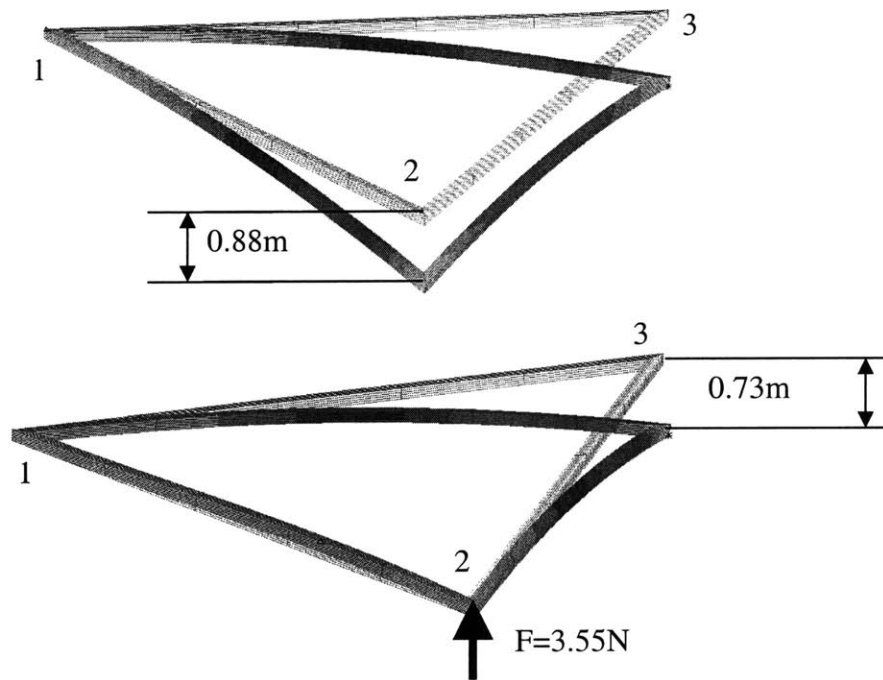


Figure 3.10: Assembly plan for the single connection point assembly case

The robot may apply the forces using various control strategies, both open and closed loop. The problem is somewhat akin to the task of putting one end of a long, thin strip of metal into a slot when the other end is rigidly fixed. Truss mechanics will play an important role and bending will be sensitive to direction since out-of-plane stiffness is much less as compared to in-plane stiffness. Simple closed loop strategies may not necessarily work in all cases. Some control strategies have been analyzed in detail in subsequent sections.

3.3.2 Multiple Connection Points

In this case, the small truss needs to be connected to the base truss at multiple points along each side (See Figure 3.11). This could be required, for example, in assembling a reflecting surface on to an existing framework. Truss shape is important, and hence the goal is to minimize shape error between the thermally deformed trusses. All other conditions remain the same as the single connection point case.

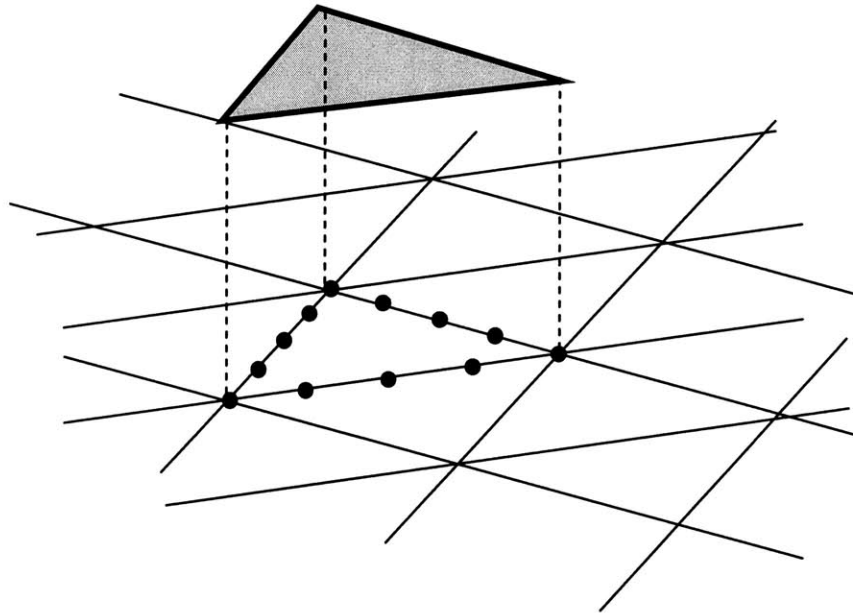


Figure 3.11: Assembly with multiple connection points

Assembly Plan

Assembly can be carried out if all the pairs of connection points are brought within a certain distance of each other specified by the joint tolerance. This can be achieved in two ways. The first method is to make one connection at a time. This is always possible since the maximum deformation is within manipulator reach. This technique requires only one robot to perform the task. However, due to the small moment arm associated with making consecutive joint connections, a large force may be required to provide the necessary moment to bend the triangular truss. This force may exceed the robot capabilities.

The second and more elegant method is to bend the entire truss to the desired shape in one step, such that the distance between the connection points is within the joint

tolerance. Given unlimited number of robots working simultaneously, this is always possible. The challenge, however, is to optimize the force locations and magnitudes to use minimum resources. Since the shape of the structure is important, the root mean square deviation of points on the structure from the desired shape is used as an error measure. The variation of this RMS deviation with increasing number of robots used to deform the structure is shown in Figure 3.12.

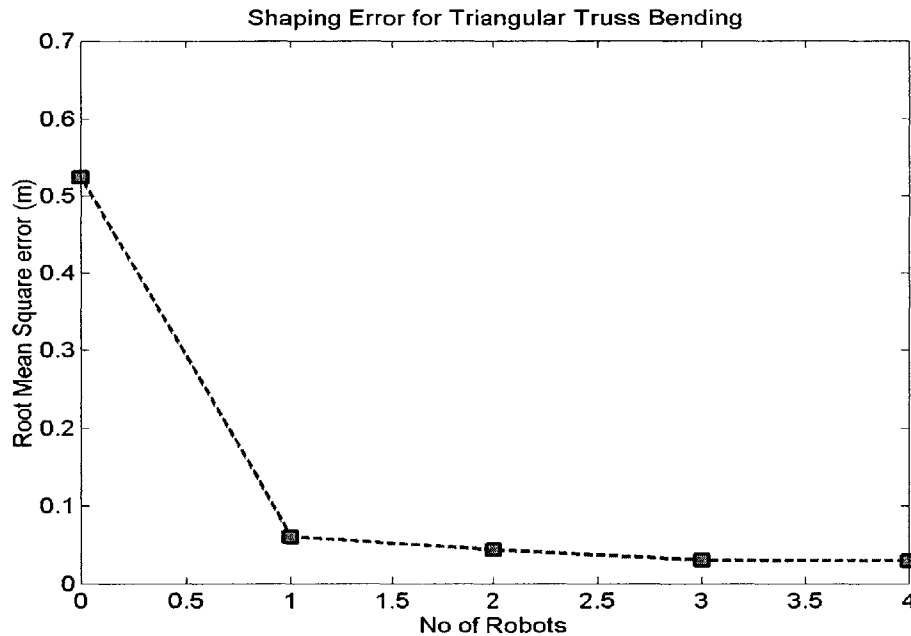


Figure 3.12: Change in shape error for triangular truss bending with number of robots

Chebyshev spacing

Thus far, it had been assumed that the location of connection points would either be equi-distant or pre-determined, and the small truss would be bent to conform to their locations. However, in some situations such as in the construction of the huge mirror for the SSPS, the shape of the individual panels that will reflect the solar radiation will be critical and should be minimally deformed. In such situations, the location of connection points themselves can be optimally determined using the Chebyshev spacing method [Hartenberg and Denavit, 1964] to minimize the shape error. A Chebyshev polynomial has the property of deviating the least from zero in an interval, amongst all same-degree polynomials with leading coefficient equal to unity. Therefore, if the connection points

on the truss are chosen to match with the accuracy points of the corresponding Chebyshev polynomial, then the shape error will be minimized. This principle has been applied to beam bending as shown in Figure 3.13.

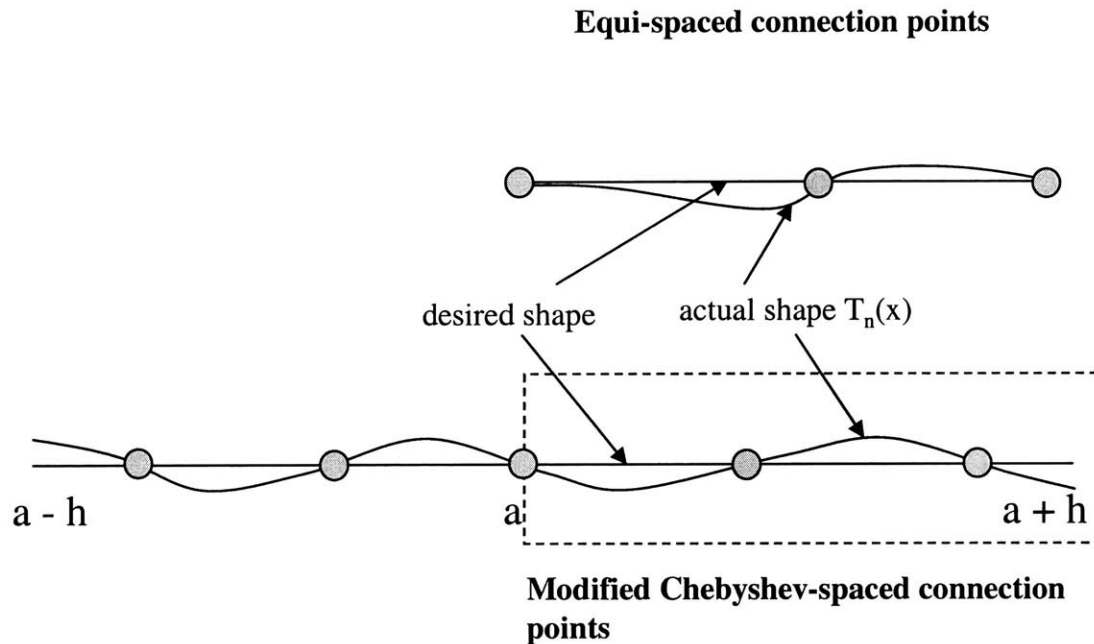


Figure 3.13: Equi-distant spacing vs Chebyshev spacing

A Chebyshev polynomial is given by:

$$T_n(x) = h^n 2^{1-n} \cos \left[n \cos^{-1} \left(\frac{x-a}{h} \right) \right] \quad (3.3)$$

where, n = number of accuracy points

The accuracy points will be the optimal location of connection points. Chebyshev spacing of accuracy points has been slightly modified to match the boundary conditions in the beam-bending case. As seen in Figure 3.14, the shape error indeed turns out to be lower for Chebyshev spacing of connection points as compared to equi-distant spacing.

Multiple connection points will ultimately affect the structural stability of the base truss. The effect of multiple connection points on structure stiffness is shown in Figure 3.15. The approximate stiffness values were computed by applying a unit force to the finite element models of the trusses in ADINA and determining the corresponding displacements.

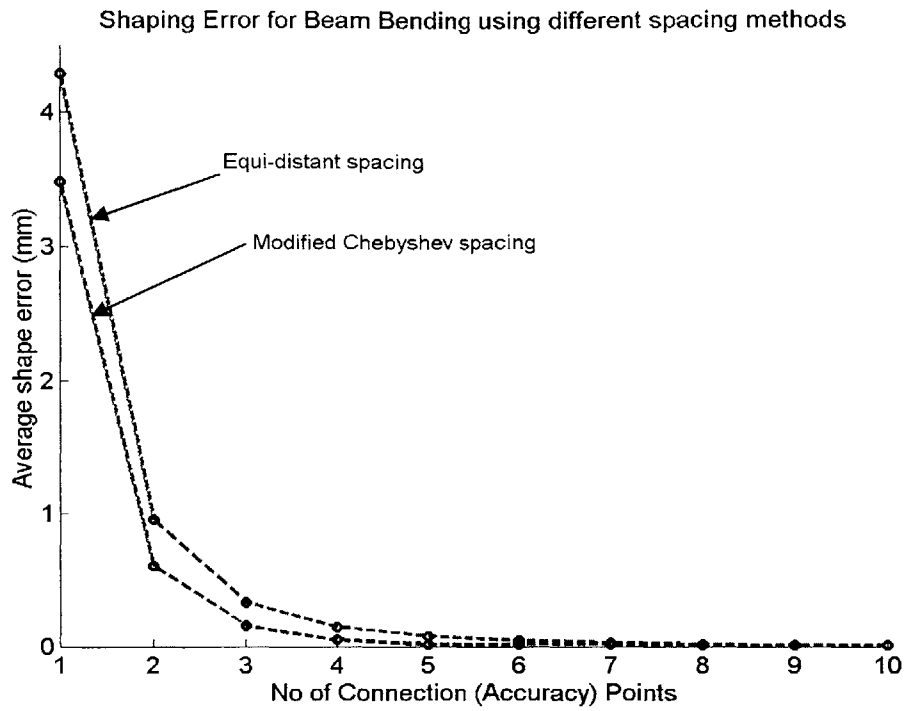


Figure 3.14: Shape error for beam bending – Equi-distant vs Chebyshev spacing

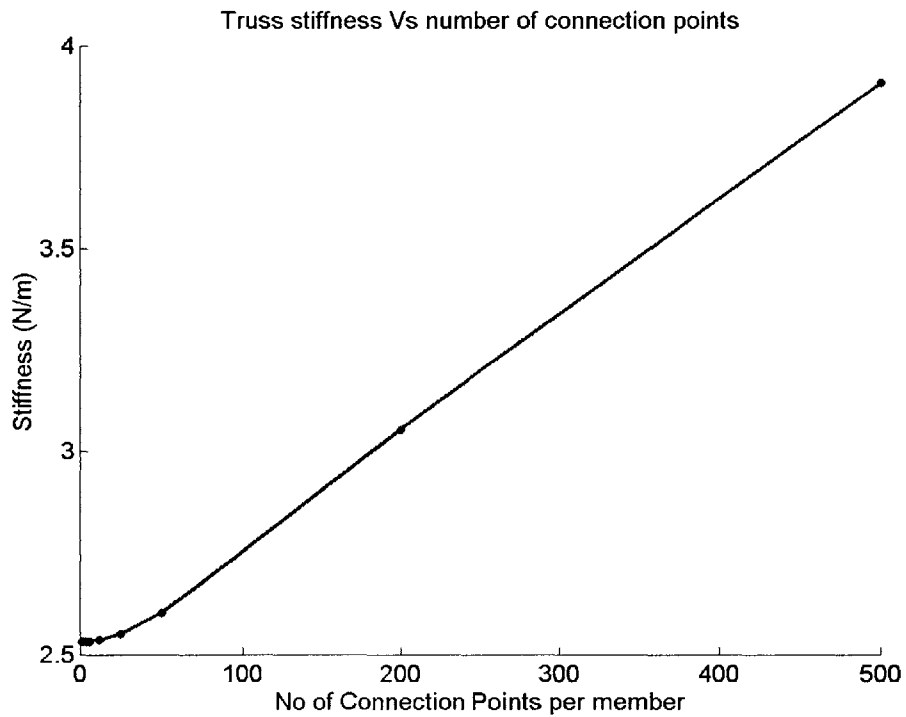


Figure 3.15: Effect of multiple connection points on truss stiffness

3.3.3 Flexible LSS

Although the base truss has been modeled as a rigid body so far, in some cases it may be as compliant as the small truss. In such a case, the flexibility of both trusses will have to be taken into account and both trusses will be deformed for the assembly process.

To compare stiffness of the base and small truss, finite element models have been created (Figure 3.16). Forces are applied at one end of the small truss with another end held rigid. The corresponding stiffness is measured as F/δ . Similar value of stiffness is measured for the same triangular truss but embedded in the base truss with corner connection points. The stiffness of the base truss in this case turns out to be greater than the small truss. However, since the base truss is huge, forces can also be applied at locations some distance away from a particular corner of the small triangular truss to deform it. It is seen that as the point of application of the force moves away from the target point of deformation on the base truss, the stiffness decreases. This implies that it may be advantageous to carry out deformation of a particular point on the base truss by applying forces several beam lengths away on the base truss (See plot in Figure 3.16). Additional factors need to be considered here especially the problem of controlling non-collocated actuators.

In the previous scenarios it was assumed that the base truss would absorb all unbalanced forces and moments. In this scenario, the dynamics of the entire structure (base truss and small truss) must be analyzed immediately after the connector has rigidly secured the joint. The elastic energy stored in the beam will be quickly transferred to the base truss when the robot releases the structure. This transfer of energy can be modeled as an impulsive force equivalent to the force required for bending the truss. The displacement of the mating point immediately after the connection has been made under the action of this impulsive force and undamped conditions is shown in Figure 3.17. Although the amplitude of this vibration will typically be small, there will be some very low frequency components that may be difficult to damp out.

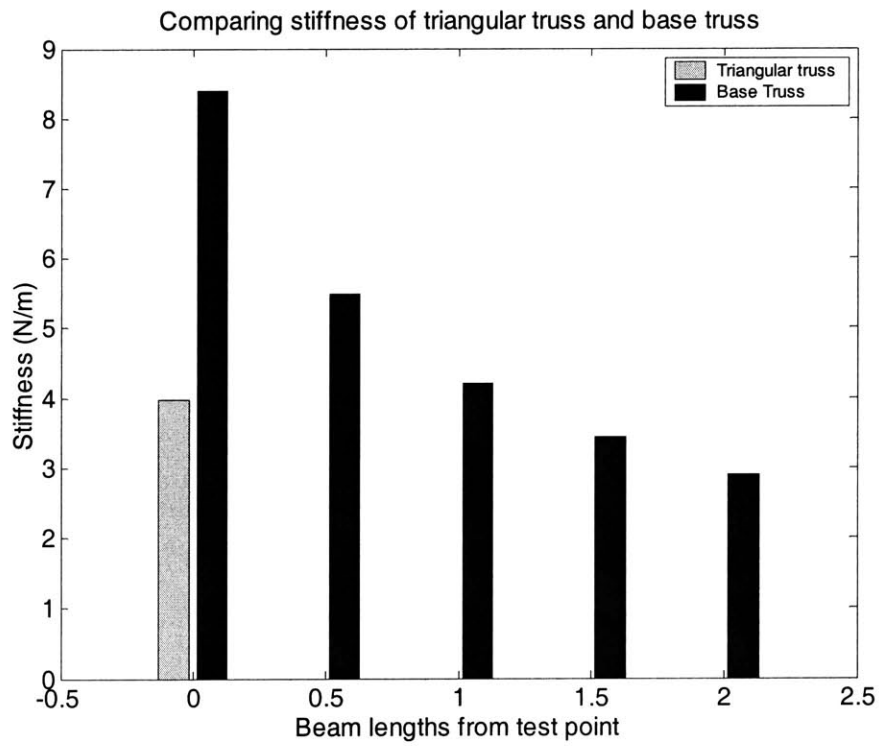
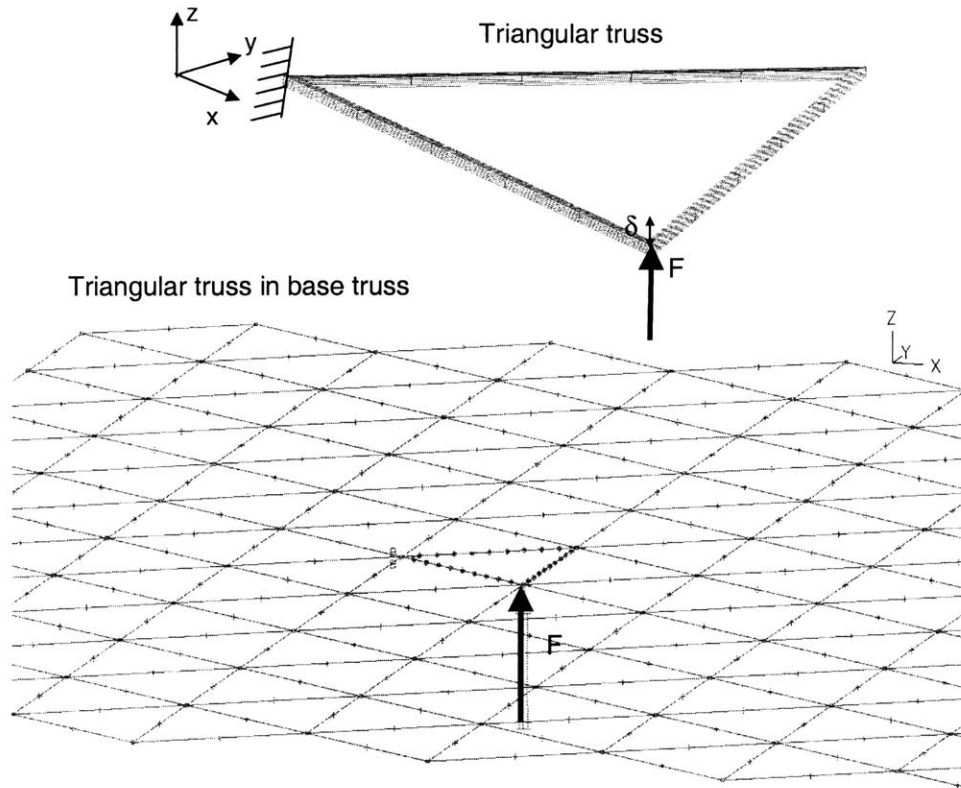


Figure 3.16: Comparing stiffness of triangular truss and base truss

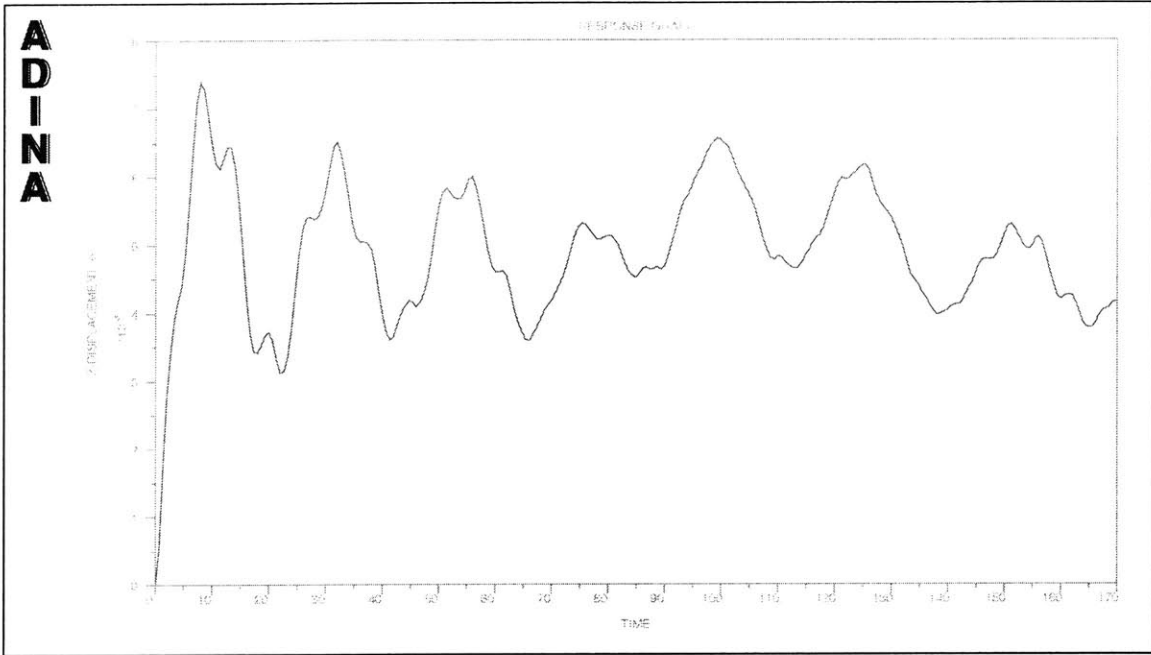


Figure 3.17: Vibrations of the mating point after connection

3.4 Large Scale Deformation Scenarios

3.4.1 Single Connection Point

Similar to the assembly scenario described in section 3.3.1, the assembly considered here involves setting up the basic framework of the truss. Hence, there is no underlying structure to grasp as a support. In the general case, factors like thermal deformation, vibration, manufacturing tolerances, etc. would contribute to the total dimensional mismatch. Robot manipulators proposed for LSS assembly, have a typical reach of about 1.5 m. Thus, any mismatch of more than 3 m will be out of reach of a robot having two such manipulators. As shown in Figure 3.18, connection only needs to be made at the corners of the triangular truss with the framework. The other scenario conditions regarding robot characteristics and joint tolerances remain the same as in section 3.3.1.

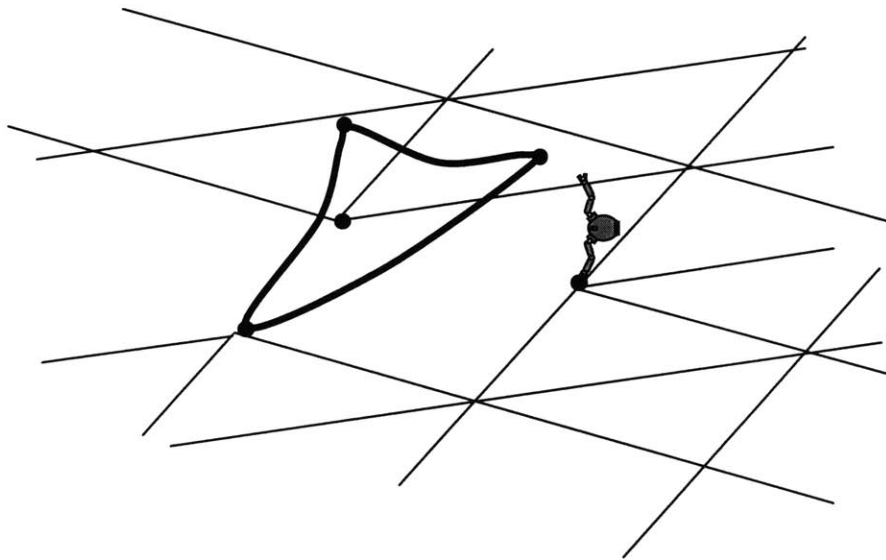


Figure 3.18: Assembly for large scale deformation with single connection point

Assembly Plan

If the base truss stiffness and mass are such that all reaction forces and vibrations will be absorbed by the base truss, then the solution to this problem is simply to replace the manipulator action used in the assembly problem for section 3.3.1 by thrusters. Finite element models of the thermally warped base truss and small truss are created as before. These are used in determining the magnitudes and direction of the forces to be applied by thrusters to carry out the static deformation.

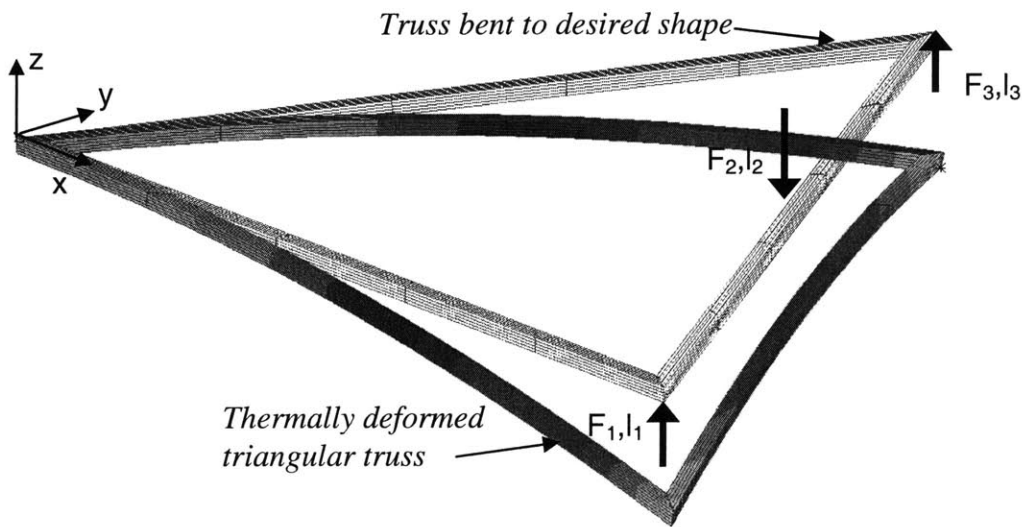


Figure 3.19: Finite Element Model of Small Truss Bent using Thrusters

Since thrusters are used, forces can be applied anywhere along the truss members. It follows that for given bending properties, there will be an optimal location of force application for which the error between the desired shape of the truss and the bent shape is minimized. For a single force applied along a triangular truss at different points, this RMS shape error is plotted in Figure 3.20. All bending analyses are carried out using finite element models in ADINA (see Figure 3.19). The plot shows that the optimal location for bending the truss with a single force would be at $L = 300$ m along the sides of the truss (see length convention in Figure 3.20), which turns out to be the mid point with respect to the fixed end.

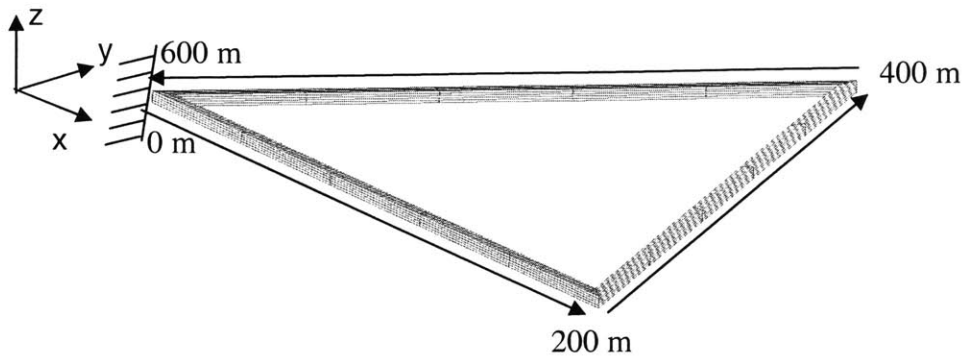
The scenario becomes more complex if the assumption about the base truss compliance is removed, i.e. the base truss is now free-floating in space and any unbalanced forces and torques will affect the stability and motion of the entire structure.

As before, the first joint would be connected without significant forces being required. Two approaches can be used to overcome the problem of the mismatch being out of range of the robots:

(i) Connect one joint of the small truss at a time, bending one side only. This could be carried out by the combined force application of multiple robots using thrusters. Since the entire system is free-floating, there must be no unbalanced forces and moments acting on the system. All forces would be in the vertical plane containing the side of the small truss under consideration as shown in Figure 3.19. Thus the following equations would have to be satisfied:

$$\sum F_z = 0, \sum M_{\text{about axis } \perp \text{ beam}} = 0 \quad (3.4)$$

As there are two constraint equations, a minimum of 3 forces are required to perform this task. This implies that a minimum of three robots are required.



Length convention for triangular truss

Overall RMS deviation of triangular truss from desired shape - Single force application
Using data from Finite Element Analysis

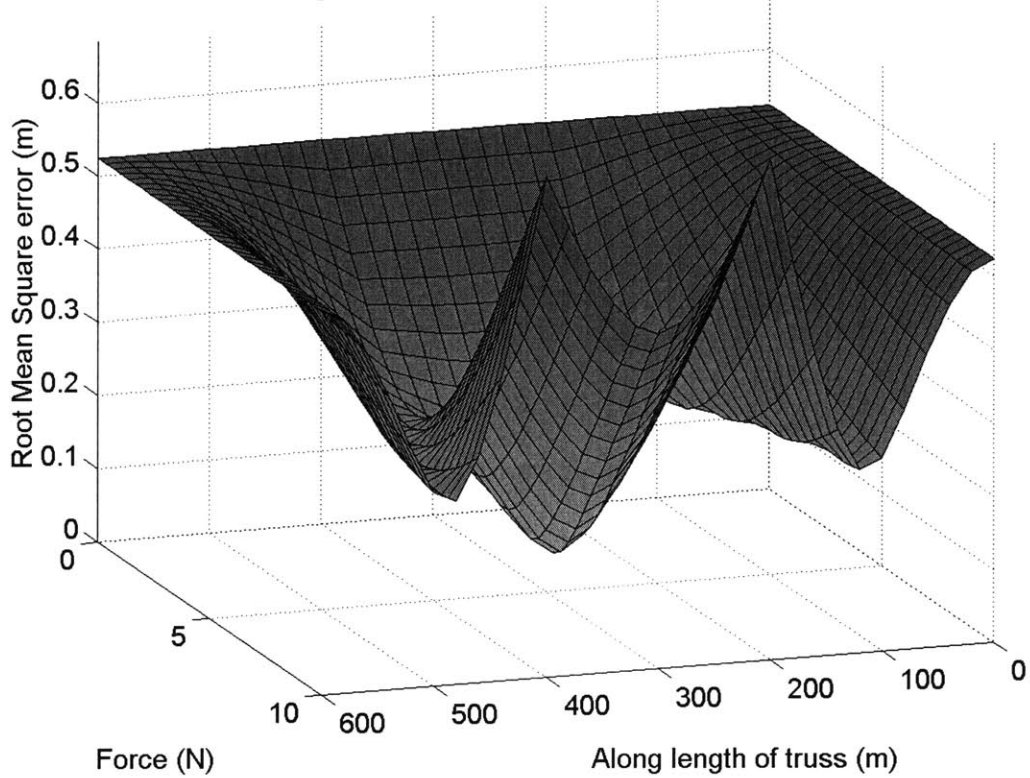


Figure 3.20: Variation in shape error of triangular truss for force application anywhere on the truss

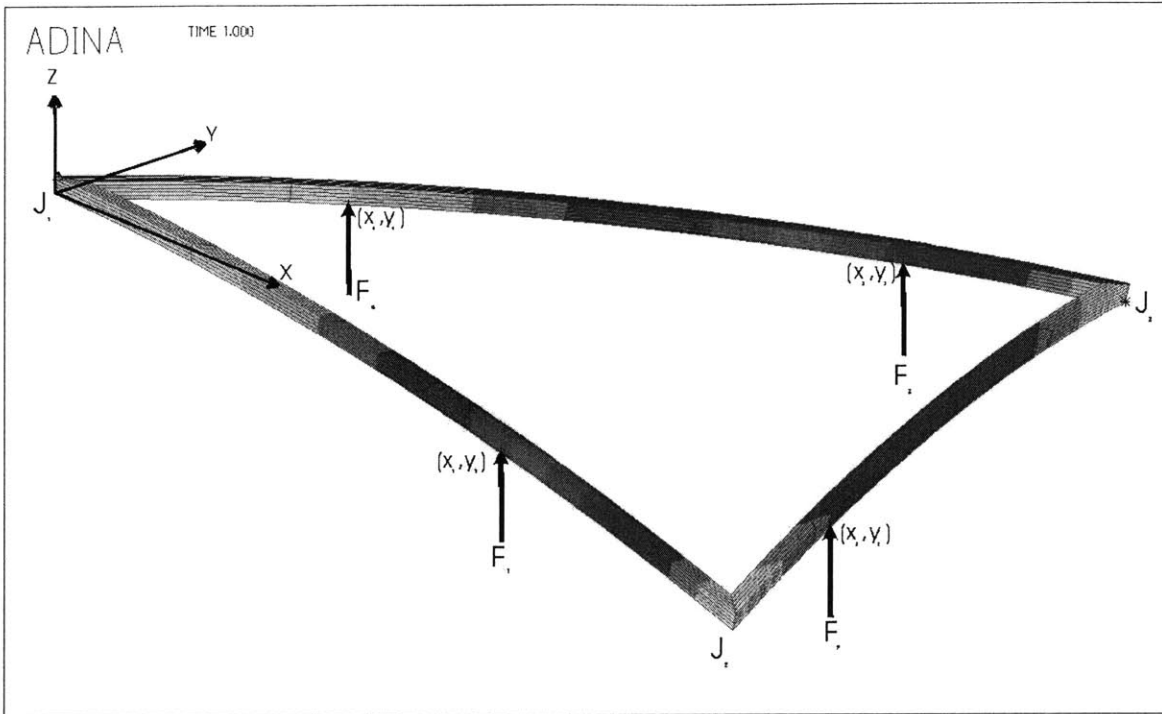


Figure 3.21: Simultaneous deformation for assembly using multiple robots

(ii) Connect both joints simultaneously by bending all three sides of the truss at the same time using multiple robots. The condition for no unbalanced forces and moments would imply that:

$$\sum F_z = 0, \sum M_x = 0, \sum M_y = 0 \quad (3.5)$$

The three constraint equations require a minimum of 4 robots to carry out this approach.

Figure 3.21 shows an assembly approach for this method. The above conditions translate to the following constraint equations:

$$\begin{aligned} F_1 + F_2 + F_3 + F_4 &= 0 \\ F_1 x_1 + F_2 x_2 + F_3 x_3 + F_4 x_4 &= 0 \\ F_1 y_1 + F_2 y_2 + F_3 y_3 + F_4 y_4 &= 0 \\ -F_{thruster, \max} < F_1, F_2, F_3, F_4 < F_{thruster, \max} \end{aligned} \quad (3.6)$$

The forces are also restricted to be applied on the truss which creates additional constraints for x_n, y_n .

In both approaches, the configurations of robots applying different forces at different points on the truss needs to be optimized. One method for optimization is to exhaustively search through all possible combinations of forces and their application points, subject to the constraining equations and by applying these forces to the finite element model. The forces are further restricted to be applied only at certain points on the truss corresponding to the nodes in the FE model. A cost function based on the error of the joint with respect to the target (obtained from FE analysis) and the magnitude of the forces required is minimized. An optimal set of forces is determined for both approaches using representative numbers for different parameters.

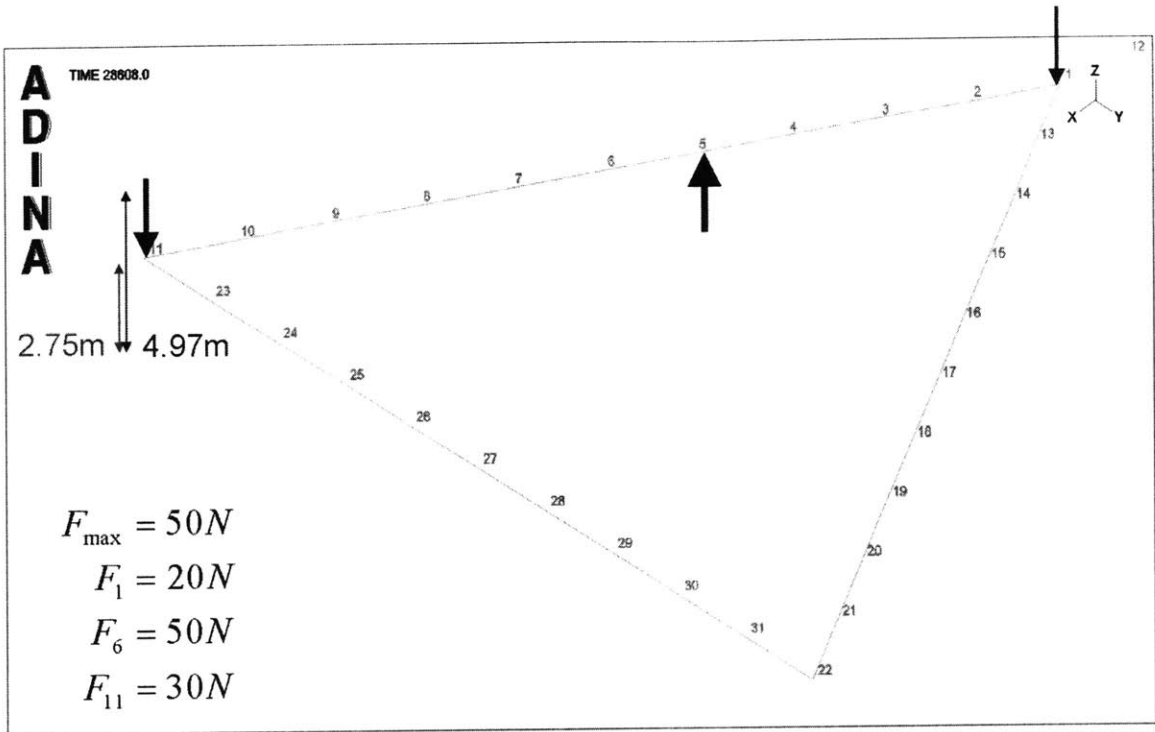
Figure 3.22 shows each side of the deformed small truss divided into 10 sections and 11 nodes. The initial deformation at each corner is 4.97m. The optimal force combination turns out to be

$$F_1 = -0.6F, F_6 = F, F_{11} = -0.4F$$

where, F_n is the force applied at the n th node and F is the maximum force that can be applied by the thrusters

Figure 3.22 also shows a scatter plot of the position error for different force combinations. The value of F used here is 50 N. The forces are discretized in 5 N intervals within the range of force application (-50 to 50 N in this case). The least distance between the joint and target point that could be achieved with this force range turns out to be 2.75m.

Although this is the minimum separation that can be achieved given the deformation and thruster capabilities, it is still far outside the tolerance range of the joint connectors (0.02 m). In such a situation, it is possible to use the cooperative action of robots in the process. Thrusters may not be able to exert very large forces to deform the small truss completely into place. Instead, thrusters might only bend the truss until it gets within the reach (3 m in this case) of another robot waiting at the mating point, ready to grip its corner.



Position error for different combinations of forces
Range: -50 to 50 N Interval: 5 N

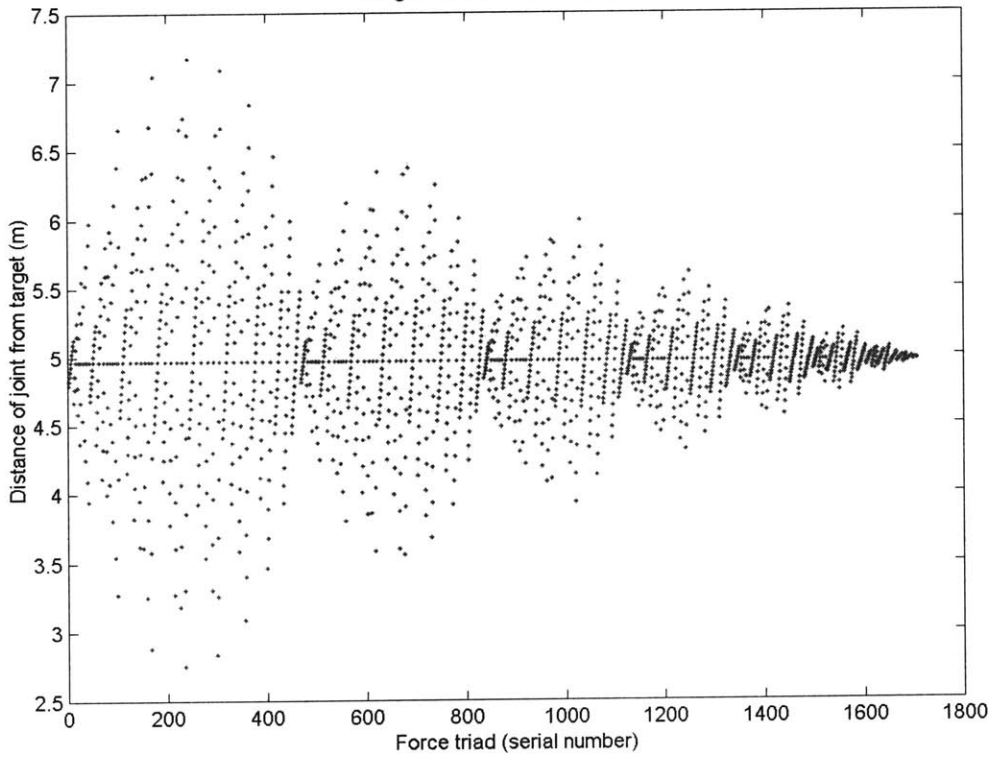


Figure 3.22: Determining Optimal Force Combination for Bending Small Truss

3.4.2 Multiple Connection Points

It has been seen in the previous section that for situations involving large dimensional mismatch, thrusters must be used to deform the truss prior to assembly. If assembly is performed onto an existing framework where typically there would be many connection points along each beam (Figure 3.23), the shape of the truss will be important, not just the deformation at the corner points. The goal would be to minimize the shape error while bending the truss. This problem is similar to the one discussed in section 3.3.2 with the additional feature of large-scale deformation.

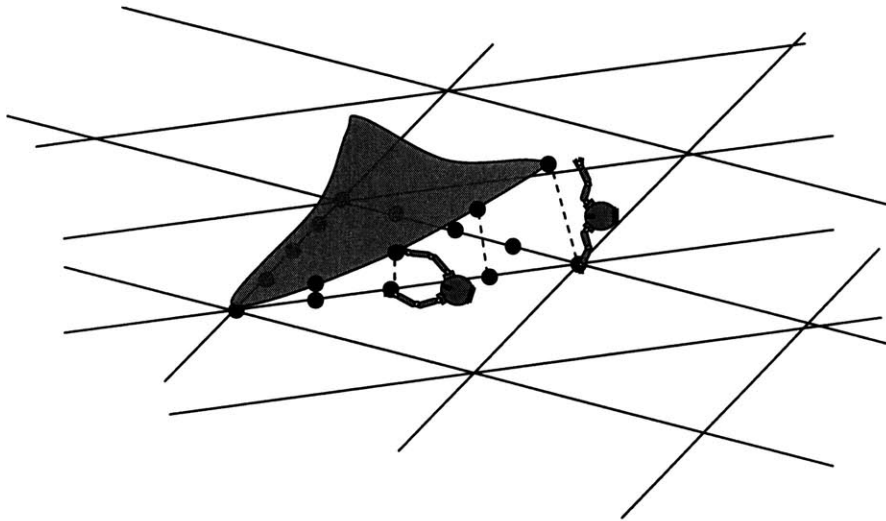


Figure 3.23: Assembly with multiple connection points

Assembly Plan

In assembly scenarios where a specified number of connections need to be made, thermally deformed structures have to be physically bent so as to get the connection points within grasping distance of each other. Again, two approaches are possible:

- (i) The first approach would be to use the fact that the small truss would be connected at least to one point on the base truss. From this point, the robot could simply use its manipulators at a point where it is able to grasp both trusses and progressively perform the connections. Figure 3.23 shows this ‘button-down’ approach. The analysis for this approach would be similar to the analysis discussed in section 3.3.1, however with one important caveat. Since the forces would be applied closer to the fixed connection point than before, the advantage of having a

significantly large moment arm (200 m in this case) is lost. For a simple beam, the beam bending relationship for forces acting in the transverse direction is given by

$$y = \frac{FL^3}{3EI} \quad (3.7)$$

where, y is the displacement at distance L from the fixed end of the beam where force F is applied. This shows that the force required for a given displacement varies inversely as the as the cube of the distance from the fixed end. The force required quickly increases beyond the capabilities of the robot manipulators.

(ii) The second approach would be to use thrusters for deformation. Since they can be applied anywhere along the sides of the truss, their placement could take advantage of the moment arm. The challenge here is to determine the minimum number of robots required for this task. A cost function based on the forces and deformation was set up and genetic algorithm based optimization was carried out for determining the optimal locations and force magnitudes for a given number of connection points. Figure 3.24 shows the minimum number of robots used to successfully perform all connections as a function of the number of connection points per beam. The results are shown for a single beam as well for a triangular truss. Figure 3.25 shows the reduction in position error of the connection points for the triangular requiring connections at two points per side. Note that with 5 robots the error becomes zero because the all the connection points are brought within 0.02 m of each other by suitably bending the truss.

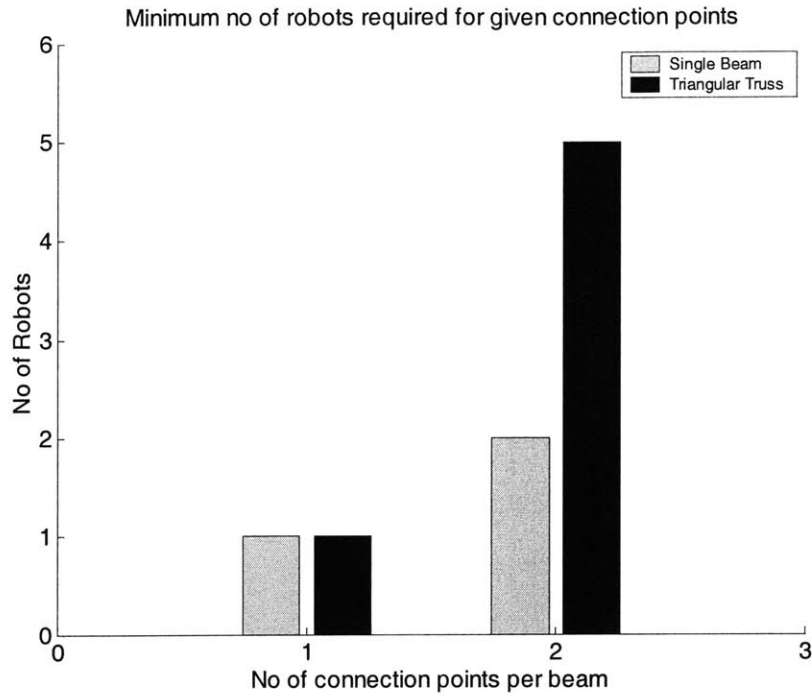


Figure 3.24: Minimum number of robots required to connect at given connection points on each beam of the truss

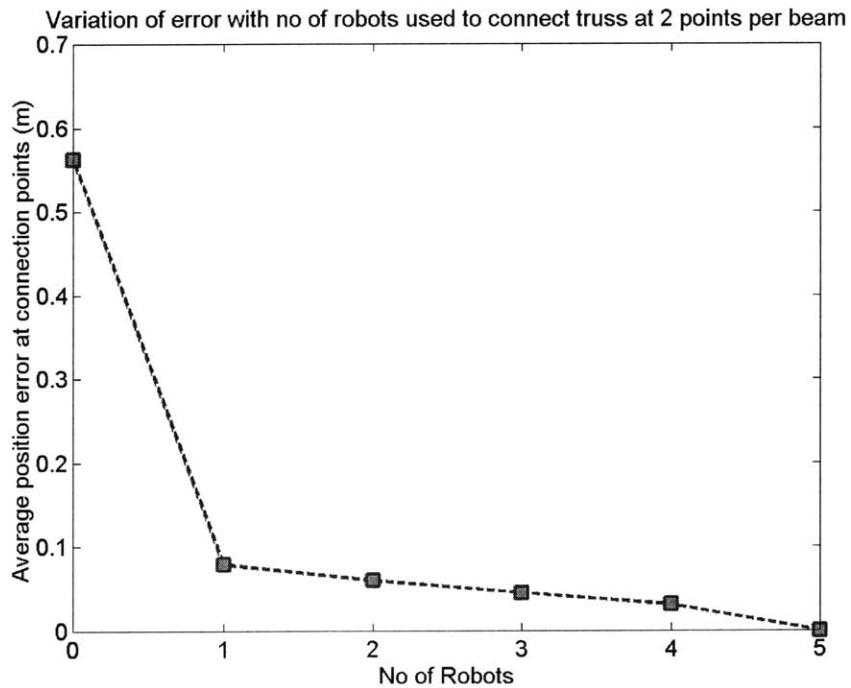


Figure 3.25: Variation of error with increasing number of robots used for assembly (2 connection points per beam)

CONCLUSIONS AND FUTURE DIRECTION

4.1 Conclusions

The main focus of this work was to identify potential problems that may be associated with future large space structure construction missions and develop methods to mitigate these problems.

Chapter 1 explained the concept of Large Space Structures and reviewed work done so far. It also introduced the problem of large space structure assembly for space solar power generation.

Chapter 2 developed a model for the large space structure assembly process. Assumptions were made about the assembly scenarios and structural analysis was carried out on the large space structure using finite element models. The assembly problem was presented and methods for forced assembly were developed.

Chapter 3 developed optimization tools for the assembly process including a genetic algorithm-based quasi-static assembly planner. Some representative assembly scenarios involving small scale deformation were analyzed and assembly plans recommended for them. This chapter also dealt with the assembly scenarios involving large scale deformation. The use of thrusters for such assembly problems was discussed and optimal assembly plans were presented.

4.2 Future Direction

The research in the area of large space structure construction is at a nascent stage but extremely challenging nevertheless. There is tremendous opportunity to identify new avenues of research in this area. Some of them have been listed below:

Multiple Robot Manipulation and Control

Since most of the assembly tasks involve the use of multiple robots it is essential to develop techniques for their manipulation and control. Additional factors like communication delays and coordinated thruster/manipulator action need to be taken into account. The communication delay may be modeled as a transport lag in the preliminary analysis.

Compensation for Dimensional Mismatch

A number of different methods can be used to compensate for dimensional mismatch apart from the brute force method discussed in the thesis. These are:

- Reconfiguration – Instead of applying external forces to the truss to deform it, the truss could be embedded with thousands of small actuators in a distributed network that would reconfigure it to the desired shape.
- Timed assembly – For a structure oscillating with a very low frequency and large amplitudes, assembly could be performed during the part of the cycle when dimensional mismatch is least. Accurate sensing methods would have to be developed to determine the period and nature of the oscillations as well as to estimate the current state of the structure.
- Damping of vibrations – For a structure causing problems in assembly due to vibration, sufficient damping elements could be embedded in the structure to damp out the vibrations. In such a scenario, the location of the damping elements would be important and would have to be optimized for a given configuration.
- Smart connectors – The assembly problem due to mismatch can be completely offset by an intelligent design of latching mechanisms that have degrees of freedom in 3 dimensions. These mechanisms could have sensors to detect the magnitude of the mismatch and actuators to perform the connection without external help. These would

definitely be very expensive and may not be a viable option. Nevertheless, they do pose an interesting design and development problem.

Transportation

Large space structure construction would entail the overall transportation of components from the transport shuttle to the construction site and also local transportation of structural elements in and around the construction site. The objective here would be to develop control algorithms to carry out this task. The constraints involved would be:

- Using multiple, free-flying robots, operating in a cooperative manner
- Transportation time
- Fuel/Energy consumption
- Physical system constraints – flexible beams and trusses
- Vibration suppression/mitigation
- Safety

The basic transportation problem is to transport a structure from rest-to-rest using thrusters with the least possible residual vibrations (See Figure 5.1). Input shaping methods or jerk control methods [Muenchhof and Singh, 2003, Singh and Vadali, 1993, Singer and Seering, 1990] applied to the command profile of the thrusters could be used here to determine the location of force application.

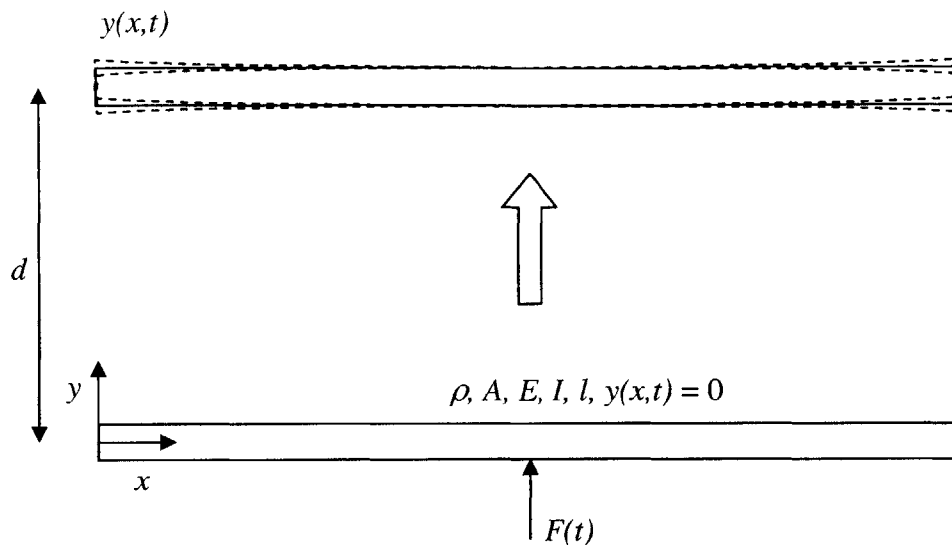


Figure 4.1: The LSS transportation problem – minimize vibrations and energy loss

The forcing function $F(x,t)$ needs to be expressed in a form that will make it possible for these equations to be solved using numerical methods in MATLAB. This problem can be looked upon as an optimization problem where the total energy of the system at the final point needs to be minimized. The optimal solution could then be tested in simulations with finite element models to check the validity of the analytical model. This vibration model set up in ADINA could directly be used in this analysis.

REFERENCES

- Adelman, H. M., and Shore, C. P., 'Thermal Analysis Considerations for Large Space Structures', *NASA Conference Publication – Modeling, Analysis, and Optimization Issues for Large Space Structures*, NASA, Washington, DC, USA, 1983, pp 123-147
- Agarwal, B. N., and Treanor, K. E., 'Shape Control of a Beam Using Piezoelectric Actuators', *Smart Materials and Structures*, Vol 8, No 6, December 1999, pp 729-739
- Brown, W.C., 'The History of Power Transmission by Radio Waves', *IEEE Transactions on Microwave Theory and Techniques*, Vol MTT-32, No 9, September 1984, pp 1230-42
- Casella, F., Locatelli, A., and Schiavoni, N., 'Modeling and Control for Vibration Suppression in a Large Flexible Structure With Jet Thrusters and Piezoactuators', *IEEE Transactions on Control Systems Technology*, Vol 10, No 4, July 2002, pp 589-599
- Coppa, A. P., 'Robotic Assembly of Truss Beams for Large Space Structures', *Journal of Spacecraft and Rockets*, Vol 32, No 4, July-August 1995, pp 680-685
- Dick, R. E., Faddis, T. N., and Barr, B. G., 'Erectable Truss Hardware for Large Space Structures', *Proceedings of the 4th International Conference on Engineering, Construction, and Operations in Space*, 1994, pp 414-422
- Duke, M. B., Ignatiev, A., Freundlich, A., Rosenberg, S., and Makel, D., 'Silicon PV Cell Production on the Moon', *Journal of Aerospace Engineering*, Vol 14, No 2, April 2001, pp 77-83

- Fiengold, H., and Carrington, C., 'Evaluation and Comparison of Space Solar Power Concepts', *53rd International Astronautical Congress*, Houston, Texas, October 2002
- Glaser, P., 'Evolution of the Satellite Solar Power Station (SSPS) Concept', *Journal of Spacecraft and Rockets*, Vol 13, No 9, Sep 1976, pp 573-576
- Grey, J., 'Technical Assessment of Space Solar-Power Research Program', *Journal of Aerospace Engineering*, Vol 14, No 2, April 2001, pp 52-58
- Gross, D., and Messner, D., 'The Able Deployable Articulated Mast – Enabling Technology for the Shuttle Radar Topography Mission', *AEC-Able Engineering Company, Inc.*, www.aec-able.com
- Hartenberg, R. S., Denavit, J., *Kinematic Synthesis of Linkages*, McGraw-Hill Book Company, USA, 1964, pp 140-147
- Incropera, F. P., DeWitt, D. P., *Fundamentals of Heat and Mass Transfer*, 4th Edition, John Wiley and Sons, 2000, pp 680-686
- Kimura, S., and Tsuchiya, S., 'Antenna-assembly experiments using ETS-VII', *European Space Agency (Special Publication)*, No 440, 1999, pp 307-312
- Lichter, M. D., and Dubowsky, S. D., 'Estimation of State, Shape, and Inertial Parameters of Space Objects from Sequences of Range Images', *SPIE's International Symposium on Optical Technologies for Industrial, Environmental, and Biological Sensing*, Providence, RI, October 2003
- Madhani, A., and Dubowsky, S., 'The Force Workspace: A Tool for the Design and Motion Planning of Multi-Limb Robotic Systems', *Transactions of the ASME*, Vol 119, June 1997, pp 218-224
- Malla, R. B., Nash, W. A., and Lardner, T. J., 'Thermal Effects on Very Large Space Structures', *Journal of Aerospace Engineering*, Vol 1, No 3, July 1988, pp 171-180

- Mankins, J. C., 'A Technical Overview of the "Sun Tower" Solar Power Satellite Concept', *Acta Astronautica*, Vol 50, No 6, March 2002, pp 369-377
- Mankins, J. C., 'Space Solar Power: A Major New Energy Option?', *Journal of Aerospace Engineering*, Vol 14, No 2, April 2001, pp 38-45
- Mankins, J. C., 'Space Solar Power: An Assessment of Challenges and Progress', *Journal of Aerospace Engineering*, Vol 14, No 2, April 2001, pp 46-51
- Mankins, J. C., 'The Promise and the Challenge of Space Solar Power in the 21st Century: Picking up the Gauntlet', *53rd International Astronautical Congress*, Houston, Texas, October 2002
- Muenchhof, M., and Singh, T., 'Jerk Limited Time Optimal Control of Flexible Structures', *Transactions of the ASME – Journal of Dynamic Systems, Measurements and Control*, Vol 125(1), March 2003, pp 139-142
- National Aeronautics and Space Administration (NASA), 'Extravehicular Activity (EVA) Standard Interface Control Document', *International Space Station Program*, Johnson Space Center, Houston, Texas, February, 1997
- Oda, M., 'Space Robot Experiments on NASDA's ETS-VII Satellite – Preliminary Overview of the Experiment Results', *Proceedings of the 1999 International Conference on Robotics and Automation: ICRA 1999*, Detroit, MI, 1999
- Oda, M., 'Experiences and Lessons Learned from the ETS-VII Robot Satellite', *Proceedings of the 2000 IEEE International Conference on Robotics and Automation: ICRA 2000*, San Francisco, CA, April 2000
- O'Neill, R. F., 'Recent Developments in Thermal Analysis of Large Space Structures', *NASA Conference Publication – Modeling, Analysis, and Optimization Issues for Large Space Structures*, NASA, Washington, DC, USA, 1983, pp 33-54
- Ohkami, Y., Oda, M., 'NASDA's Activities in Space Robotics', *European Space Agency (Special Publication)*, No 440, 1999, pp 11-18

- Pignolet, G., Celeste, A., Deckard, M., and Esperet, J. P., 'Space Solar Power: Environmental Questions and Future Studies', *Journal of Aerospace Engineering*, Vol 14, No 2, April 2001, pp 72-76
- Putz, P., 'Space Robotics in Europe: A Survey', *Robotics and Autonomous Systems*, Vol 23, No 1-2, March 1998, pp 3-16
- Rule, W. K., and Thomas, F. P., 'Welded Joints for Robotic, On-Orbit Assembly of Space Structures', *Journal of Aerospace Engineering*, Vol 7, No 2, pp 209-224
- Singer, N. C., and Seering, W. P., 'Preshaping Command Inputs to Reduce System Vibrations', *Transactions of the ASME – Journal of Dynamic Systems, Measurements and Control*, Vol 115, 1990, pp 76–82
- Singh, T., and Vadali, S. R., 'Robust Time-Delay Control', *Transactions of the ASME – Journal of Dynamic Systems, Measurements and Control*, Vol 115(2A), 1993, pp 303–306
- Thornton, E. A., and Paul, D. B., 'Thermal-Structural Analysis of Large Space Structures: An Assessment of Recent Advances', *Journal of Spacecraft and Rockets*, Vol 22, No 4, July-August 1985, pp 385-393
- Ueno, H., Satoh, H., Aoki, S., Yoshida, T., Matsumoto, K., and Wakabayashi, S., 'On-Orbit Construction Experiment by Teleoperated Robot Arm', *Proceedings of the 14th International Symposium on Automation and Robotics in Construction*, 1997
- Umland, J. W., and Eisen, H., 'SRTM On-Orbit Structural Dynamics', *A Collection of Technical Papers - AIAA/ASME/ASCE/AHS/ASC Structures, Structural Dynamics and Materials Conference*, Vol 4, April 2001, pp 2997-3007
- Way, D. W., and Olds, J. R., 'Space Transfer-Vehicle Concept for Deploying Solar-Power Satellites', *Journal of Aerospace Engineering*, Vol 14, No 2, April 2001, pp 65-71

Wertz, J. R., *Spacecraft Attitude Determination and Control*, D. Reidel Publishing Company, Boston, USA, 1985

Whittaker W., Staritz P., Ambrose R., Kennedy B., Fredrickson S., Parrish J., and Urmson C., 'Robotic Assembly of Space Solar-Power Facilities', *Journal of Aerospace Engineering*, Vol 14, No 2, April 2001, pp 59-64

A

LARGE SPACE TRUSS MODEL

The analysis of a realistic assembly process requires a model of the thermally warped base truss. The thermal effects caused by heat transfer across the cross-section of the truss elements have to be simulated on the base truss. Since the heat transfer is a three-dimensional process, a 3-D finite element model of the base truss is required on which thermal loads can be applied. Such a model was developed for a truss made up of 6 smaller triangular trusses (shown in Figure A.1). It was found that even for such a small truss, thousands of nodes were required to correctly model the structural deformation. The base truss being considered would be made of hundreds of smaller triangular trusses and would have dimensions of the order of 2 km x 2 km. As a result, the finite element modeling turns out to be extremely computationally intensive for a truss of the size being envisioned.

However, modeling the mechanics of the structure is much simpler and less computationally intensive as the entire truss can be represented by beam elements with a defined cross-section. This essentially reduces the problem by one-dimension. Given the free floating nature of the truss and the fact that the total thermal deformation will be a small percentage of the total dimensions, it is assumed that the warped profile of the truss will be uniform throughout. Such a profile was determined for a small triangular truss using the finite element software ADINA. This profile was then replicated over the surface of the entire truss to generate the planar base truss model. A method to interface ADINA with MATLAB was created to achieve this. The complete base truss thus

generated was fed back to ADINA to analyze the structural deformation and effect of vibrations. Figure A.2 shows the thermally deformed base truss.

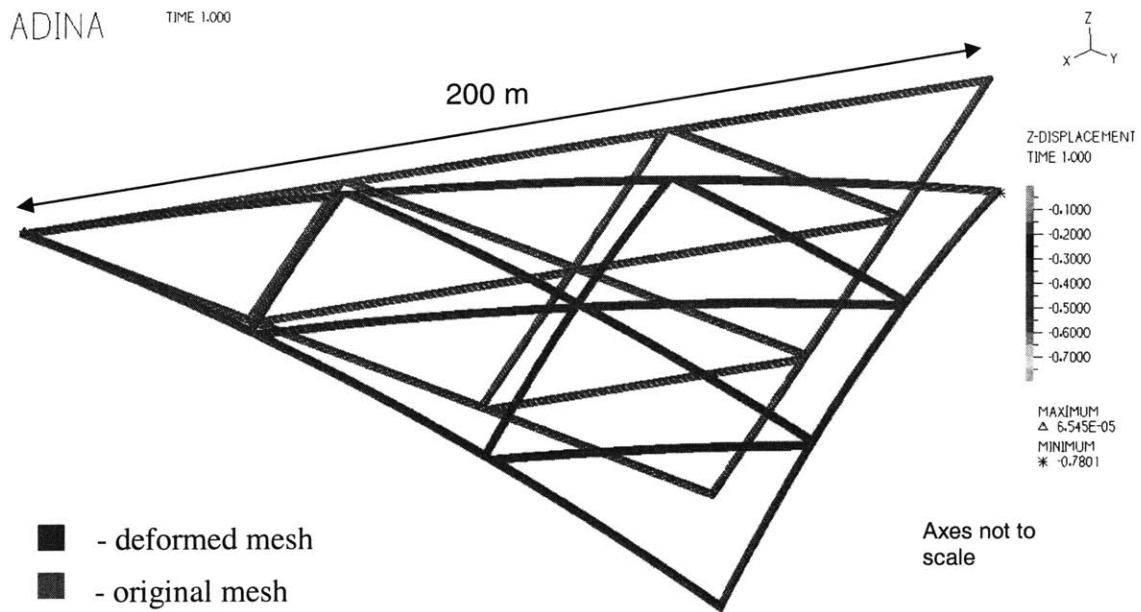


Figure A.1: Thermal deformation of a large space truss

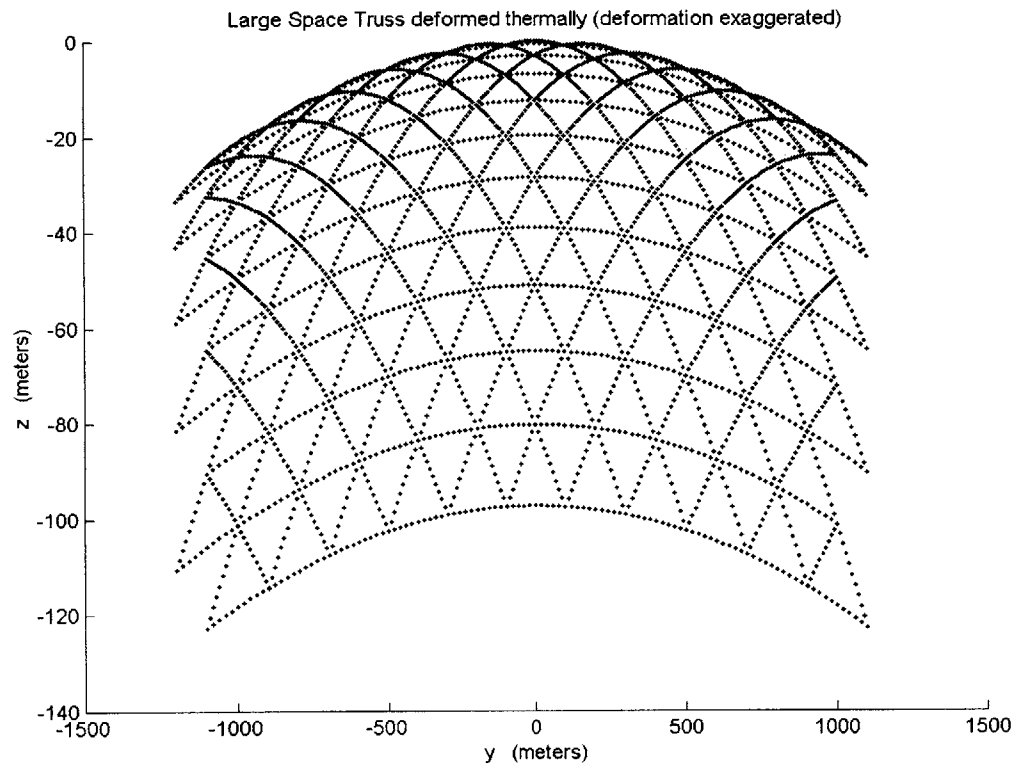
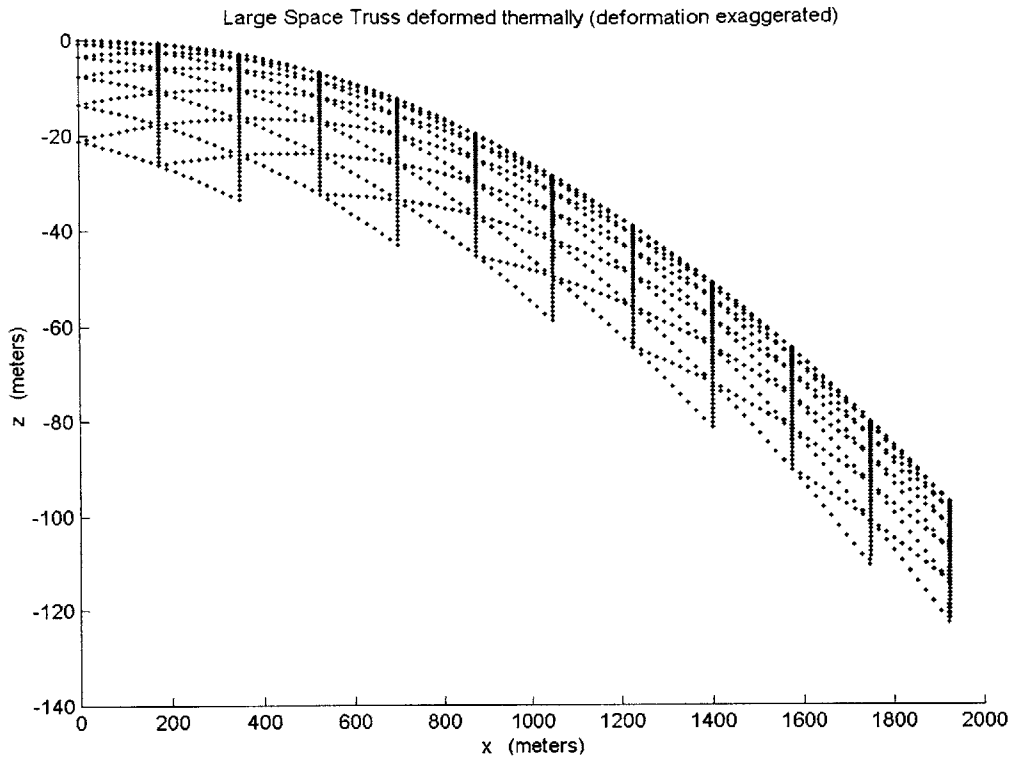


Figure A.2: Truss points generated for the large space truss in MATLAB using data obtained from thermal analysis of a smaller truss in ADINA

OPTIMAL ROBOT POSE

The optimal pose problem for a robot with two single-link arms as shown in Figure B.1 can be formulated as an optimization problem from equation 4.1 as follows:

$$\begin{aligned}
 & \max && \text{Force } F \\
 & \text{subject to} && F = f(T_1, T_2, r, \theta_1, \theta_2) \\
 & && 0 < T_1 < T_{\max} \\
 & && 0 < T_2 < T_{\max} \\
 & && 0 < r < 2L + a \\
 & && \theta_{\min} < \theta_1 < \theta_{\max} \\
 & && \theta_{\min} < \theta_2 < \theta_{\max}
 \end{aligned} \tag{B.1}$$

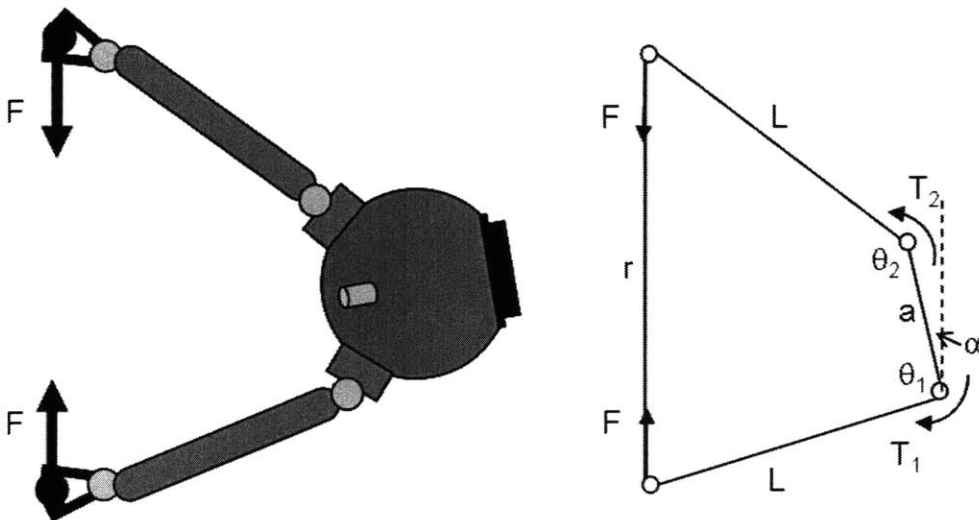


Figure B.1: Robot with two single-link arms

To determine the relationship represented by function f , the kinematic and force-torque equilibrium conditions are analyzed. The free-body diagrams of the robot arms are shown in Figure B.2.

For no unbalanced moment on the arms,

$$\begin{aligned} T_1 &= F_1 L \sin(\theta_1 + \alpha) \\ T_2 &= F_2 L \sin(\theta_2 - \alpha) \end{aligned} \quad (\text{B.2})$$

For stability of the robot body,

$$\begin{aligned} \sum F_y &= 0 \Rightarrow F_1 = F_2 \\ \sum M_z &= 0 \Rightarrow T_1 = T_2 + Fa \sin \alpha \end{aligned} \quad (\text{B.3})$$

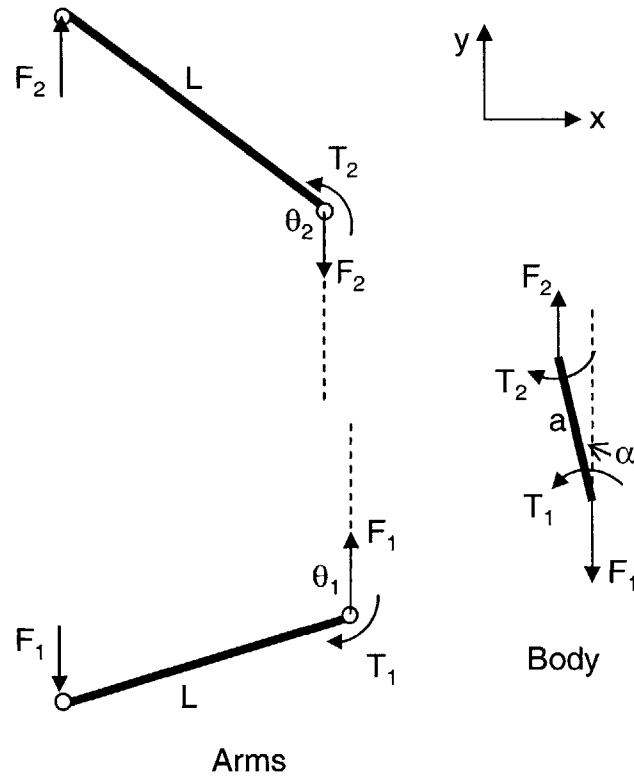


Figure B.2: Free body diagrams of the arms and body of the robot

Using the geometric configuration of the robot, for given link length L , body-width a and distance between manipulators r , the joint angles θ_1 and θ_2 can be written as a function of each other as,

$$\sin \theta_2 = \frac{(2L^2 \cos \theta_1 - 2aL) \cos \theta_2 + a^2 + 2L^2 - r^2 - 2aL \cos \theta_1}{2L^2 \sin \theta_1} \quad (\text{B.4})$$

$$\text{or, } \sin \theta_2 = \frac{m \cos \theta_2 + n}{p}$$

Squaring both sides, using trigonometric identities and rearranging,

$$(m^2 + p^2) \cos^2 \theta_2 + (2mn) \cos \theta_2 + (n^2 - p^2) = 0 \quad (\text{B.5})$$

If a robot configuration for given parameters is possible, then this quadratic will have real roots, or

$$(2mn)^2 - 4(m^2 + p^2)(n^2 - p^2) \geq 0$$

$$\text{i.e., } m^2 + p^2 \geq n^2 \quad (\text{B.6})$$

$$\text{i.e., } 4L^2 r^2 \geq (a^2 - r^2 - 2aL \cos \theta_1)^2 \quad (\text{B.7})$$

If this condition is satisfied then θ_2 can be determined as a function of θ_1 ,

$$\cos \theta_2 = \frac{-mn \pm p \sqrt{m^2 + p^2 - n^2}}{m^2 + p^2} \quad (\text{B.8})$$

In general, two configurations will be possible for a particular value of θ_1 .

For given torque T_1 , T_2 must be given by the following to ensure stability:

$$T_2 = T_1 \frac{\sin(\theta_2 - \alpha)}{\sin(\theta_1 + \alpha)} \quad (\text{B.9})$$

$$\text{where, } \tan \alpha = \frac{L \sin \theta_1 - L \sin \theta_2}{a - L \cos \theta_1 - L \cos \theta_2}$$

Finally, force F can be expressed as a function of two independent variables, θ_1 , and T_1 :

$$F = \frac{T_1}{L \sin(\theta_1 + \alpha)} \quad (\text{B.10})$$

The optimization problem reduces to

$$\begin{aligned}
& \max \quad \text{Force } F \\
& \text{subject to } F = \frac{T_1}{L \sin(\theta_1 + \alpha)} \\
& \tan \alpha = \frac{L \sin \theta_1 - L \sin \theta_2}{a - L \cos \theta_1 - L \cos \theta_2} \\
& \sin \theta_2 = \frac{(2L^2 \cos \theta_1 - 2aL) \cos \theta_2 + a^2 + 2L^2 - r^2 - 2aL \cos \theta_1}{2L^2 \sin \theta_1} \\
& T_2 = T_1 \frac{\sin(\theta_2 - \alpha)}{\sin(\theta_1 + \alpha)} \\
& 0 < T_1 < T_{\max} \\
& 0 < T_2 < T_{\max} \\
& \theta_{\min} < \theta_1 < \theta_{\max} \\
& \theta_{\min} < \theta_2 < \theta_{\max}
\end{aligned} \tag{B.11}$$

There is another constraint imposed due to the geometric configuration of the robot which will not allow intersection of the links. This needs to be checked every time a feasible value of F is computed. For simulation purposes, the limits T_{\max} , θ_{\min} , and θ_{\max} were taken to be 10 Nm, 45° and 180° respectively taking into account the geometry of the robot body. Typical values were chosen for L (1 m), a (0.5 m) and distance between mating points a (1 m). This optimization problem was solved using standard optimization routines in MATLAB. The results obtained have been discussed in section 3.1.3.